JPL PUBLICATION 84-61

Radiation Effects in Silicon and Gallium Arsenide Solar Cells Using Isotropic and Normally Incident Radiation

B.E. Anspaugh
R.G. Downing

September 1, 1984

Prepared for

U.S. Air Force Wright Aeronautical Laboratories
Wright-Patterson Air Force Base, Ohio

Through an Agreement with

National Aeronautics and Space Administration

by

Jet Propulsion Laboratory
California Institute of Technology
Pasadena, California

JPL PUBLICATION 84-61

Radiation Effects in Silicon and Gallium Arsenide Solar Cells Using Isotropic and Normally Incident Radiation

B.E. Anspaugh
R.G. Downing

September 1, 1984

Prepared for

U.S. Air Force Wright Aeronautical Laboratories
Wright-Patterson Air Force Base, Ohio

Through an Agreement with

National Aeronautics and Space Administration

by

Jet Propulsion Laboratory
California Institute of Technology
Pasadena, California

The research described in this publication was carried out by the Jet Propulsion Laboratory, California Institute of Technology, and was sponsored by the U.S. Department of the Air Force and the National Aeronautics and Space Administration.

ABSTRACT

Several types of silicon and gallium arsenide solar cells have been irradiated with protons with energies between 50 keV and 10 MeV at both normal and isotropic incidence. Damage coefficients for maximum power relative to 10 MeV were derived for these cells for both cases of omnidirectional and normal incidence. The damage coefficients for the silicon cells were found to be somewhat lower than those quoted in the Solar Cell Radiation Handbook published by the Jet Propulsion Laboratory in 1982. These values were used to compute omnidirectional damage coefficients suitable for solar cells protected by coverglasses of practical thickness, which in turn were used to compute solar cell degradation in two proton-dominated orbits. In spite of the difference in the low energy proton damage coefficients, the difference between the Handbook prediction and the prediction using the newly derived values was negligible. Damage coefficients for GaAs solar cells for short circuit current, open circuit voltage, and maximum power were also computed relative to 10 MeV protons. They were used to predict cell degradation in the same two orbits and in a 5600 nmi orbit. The performance of the GaAs solar cells in these orbits was shown to be superior to that of the Si cells.

ACKNOWLEDGMENTS

The authors take pleasure in acknowledging the tremendous help in this work by Tetsuo Miyahira and Robert Weiss, who supported the construction and operation of the irradiation chamber and omnidirectional fixture and who recorded all the I-V curves.

CONTENTS

I. INTRODUCTION 1

II. EXPERIMENTAL TECHNIQUES 2

III. DISCUSSION AND RESULTS 5

IV. CONCLUSIONS 17

REFERENCES 18

APPENDIX 61

Figures

1. Schematic of Proton Irradiation Chamber 19

2. Cam Mechanism for Producing Simulated Omnidirectional Isotropic Irradiations 20

3. Particle and Energy Dependence of Silicon P_m Degradation . . 21

4. Particle and Energy Dependence of GaAs P_m Degradation . . . 22

5. Particle and Energy Dependence of GaAs I_{sc} Degradation . . . 23

6. Particle and Energy Dependence of GaAs V_{oc} Degradation . . . 24

7. P_m Normal Incidence Damage Coefficients for Silicon Solar Cells 25

8. I_{sc} Degradation vs Omni and Normal Incidence, 10 MeV Proton Fluence 26

9. V_{oc} Degradation vs Omni and Normal Incidence, 10 MeV Proton Fluence 27

10. P_m Degradation vs Omni and Normal Incidence, 10 Mev Proton Fluence 28

11. I_{sc} Degradation vs Omni and Normal Incidence, 1 MeV Proton Fluence 29

12. V_{oc} Degradation vs Omni and Normal Incidence, 1 MeV Proton Fluence 30

13. P_m Degradation vs Omni and Normal Incidence, 1 MeV Proton Fluence 31

14. Comparison of Handbook P_m Damage Coefficients with Experiment 32

15. Omnidirectional Damage Coefficient Calculation for Protons which Penetrate Coverglass and Solar Cell 33

16. Omnidirectional Damage Coefficient Calculation for Protons which Stop in the Solar Cell 34

17. Experimental and Computed P_m Omnidirectional Damage Coefficients for Silicon Solar Cells 35

18. Experimental and Computed P_m Solar Cell Degradation by 300 keV Protons 36

19. P_m Degradation of Vertical Junction Solar Cells by 0.2 and 1.0 MeV Protons 37

20. P_m Degradation of BSF Solar Cells by 1.0 and 10 MeV Protons 38

21. I_{sc} Degradation of GaAs Solar Cells for 50 keV Protons . . . 39

22. V_{oc} Degradation of GaAs Solar Cells for 50 keV Protons . . . 40

23. P_m Degradation of GaAs Solar Cells for 50 keV Protons 41

24. I_{sc} Degradation of GaAs Solar Cells for 1 MeV Protons 42

25. V_{oc} Degradation of GaAs Solar Cells for 1 MeV Protons 43

26. P_m Degradation of GaAs Solar Cells for 1 MeV Protons 44

27. I_{sc} Degradation of GaAs Solar Cells for 10 MeV Protons . . . 45

28. V_{oc} Degradation of GaAs Solar Cells for 10 MeV Protons . . . 46

29. P_m Degradation of GaAs Solar Cells for 10 MeV Protons 47

30. Normal Incidence P_m Damage Coefficients for Si and GaAs . . . 48

31. Normal and Omni I_{sc} Damage Coefficients for GaAs 49

32. Normal and Omni V_{oc} Damage Coefficients for GaAs 50

33. Normal and Omni P_m Damage Coefficients for GaAs 51

34. Proton Integral Fluence Spectra for 1000 nmi and 3000 nmi Circular Orbits 52

35. Proton Integral Fluence Spectra for a 5600 nmi Circular Orbit 53

36. Computed Si Solar Cell P_m Degradation in 1000 nmi and 3000 nmi Orbital Proton Environments. 54

37. Computed Electrical Parameter Degradation of GaAs Solar Cells in a 1000 nmi Circular Orbit 55

38. Computed Electrical Parameter Degradation of GaAs Solar Cells in a 3000 nmi Circular Orbit 56

39. Computed Electrical Parameter Degradation of GaAs Solar Cells in a 5600 nmi Circular Orbit 57

40. Computed Si and GaAs Solar Cell P_m Degradation in 1000 nmi and 3000 nmi Orbital Proton Environments 58

41. Computed Si and GaAs Solar Cell P_m Degradation in a 5600 Orbital Proton Environment 59

42. Computed Si and GaAs Solar Cell P_m Degradation vs Time in a 5600 nmi Orbit 60

Table

1. Scattering Foils Used and Their Effect on the Proton Beams . 3

SECTION I

INTRODUCTION

The present concept of the use of a 1 MeV equivalent electron fluence to predict and evaluate the performance of solar cell arrays operating in the charged particle space radiation environment was developed in the late fifties and early sixties. A version of this model, suitable for use by solar array designers, was published and made available for general use in 1973 (1). It has been used extensively in the design of solar arrays since that time, and its use in predicting the behavior of panels in a wide variety of radiation environments has been quite successful. Since that time, considerable advances have been made in solar cell technology, in the understanding of the space radiation environment, and in the understanding of radiation effects. However, some instances of anomalous solar cell and solar array behavior in space have been reported. Finally, the validity, completeness, and accuracy of the 1 MeV equivalent electron fluence technique has come under question, particularly with respect to proton-dominated environments. For these reasons, a program has been initiated to obtain data and to reevaluate the use of this technique. In addition to looking at its application to silicon solar cells, the application to GaAs solar cells will be addressed.

Experiments have been performed in the proton energy range from 50 keV to 10 MeV. Samples tested include several types of Si cells and GaAs cells made with the liquid phase epitaxy (LPE) process incorporating GaAlAs windows. Omnidirectional and normal incidence data have been acquired simultaneously in all radiation exposures. The data have been analyzed and compared with the 1 MeV equivalent fluence model and the data published in the revised Solar Cell Radiation Handbook (2). Although the program is not yet complete, a number of interesting observations can be made at this time and are presented here.

SECTION II

EXPERIMENTAL TECHNIQUES

The silicon solar cells tested were 2 and 10 ohm-cm cells, 200 microns thick, with dual antireflection (DAR) coatings and aluminum back surface reflectors (BSR). The back surface field (BSF) solar cells were 10 ohm-cm, 200 microns thick with the field applied using aluminum paste. They also had dual AR coatings and BSR. The vertical junction (VJ) cells were 2.7 ohm-cm silicon, 250 to 300 microns thick, and had aluminum paste BSF, Ta_2O_5 AR coatings and grooves 75 microns deep with 16-micron-wide walls and 8-micron-wide grooves. The liquid phase epitaxy (LPE) GaAs cells, which were made by Hughes Research Laboratory (HRL), were 380 microns thick, made with GaAlAs windows $\leq$0.5 microns thick and junction depths $\leq$0.5 microns. All cells were 2 x 2 cm.

The proton irradiations were carried out at the California Institute of Technology using the 1 MeV and 12 MeV van de Graaff accelerators at the Kellogg Radiation Laboratory. An evacuated target chamber approximately 3 m long and 30 cm in diameter at the target end was coupled to one of the accelerator beam transport lines (Figure 1). Gold or titanium foils were placed near the entrance of the chamber to produce a large, uniform beam at the target plane. The intensity of the beam at the edge of a 10-cm-diameter circle in the target plane varied no more than 7% from the beam intensity at the center. This was accomplished at all energies by appropriate selection of foil thickness and material. Table 1 summarizes the important parameters related to producing large beams by use of the foils. The test cells were mounted within the 10-cm-diameter circle, with a Faraday cup located at the center. For each cell type and proton energy, six uncovered cells were

Table 1. Scattering Foils Used and Their Effect on the Proton Beams

Energy on Target (MeV)	Machine Energy (MeV)	Foil Material	Foil Thickness (microns)	Energy Straggling (MeV)	Intensity Fall-off at 2 inch Radius (I/I_o)
0.05	0.157	Ti	0.65	0.0056	0.99
0.1	0.206	Ti	0.65	0.0053	0.99
0.2	0.292	Ti	0.65	0.0048	0.97
0.3	0.379	Ti	0.65	0.0049	0.94
0.4	0.615	Au	1.19	0.013	0.99
0.5	0.698	Au	1.19	0.013	0.99
1.0	1.15	Au	1.19	0.016	0.97
3.0	4.70	Au	25.8	0.055	0.98
10.0	11.67	Au	50.4	0.093	0.93

divided into two groups of three each: one group for normal incidence irradiation, and the second group for omnidirectional irradiation. The six cells were alternately irradiated and measured to provide continuous degradation data for each cell. Two 10 ohm-cm control cells were also irradiated and measured each time: one on the omnidirectional fixture, and one on the fixed plane, to give assurance that no operational errors were made in the dosimetry.

The omnidirectional fixture (Figure 2) used the one axis $\dot{\theta} \alpha 1/\sin \theta$ isotropic simulation concept (3). The rotational motion is generated by a cam mechanism outside the test chamber. An extension of the vertical shaft shown in Figure 2 couples the rotary motion through a vacuum seal to the cells in the test chamber. This permits the omnidirectional cell group and the normal incidence cell group to be irradiated simultaneously to eliminate any possible geometric, environmental, or time-dependent errors. A Faraday cup mounted in the center of the non-rotating portion of the test plane was used to measure the proton flux.

After each interval of exposure, the cells were removed for air mass zero I-V curve measurements. At selected points of interest, spectral response measurements were also performed. The cells were not annealed after irradiation, and in most cases were measured within an hour of the irradiation. Post-irradiation measurements performed a month later indicated that some silicon cells had recovered as much as 4% of their initial power, so the present measurements may be considered to slightly overestimate degradation rates seen in space on a solar panel running at elevated temperature. Room temperature annealing of the GaAs cells after one month was negligible. Isochronal annealing studies are planned for these cells in the future.

SECTION III

DISCUSSION AND RESULTS

Figure 3 illustrates the degradation of 10 ohm-cm, 200-micron-thick silicon solar cells with DAR and BSR after irradiation by protons and electrons of various energies. In order for the 1 MeV equivalent electron fluence concept to be valid, these degradation curves must be parallel to each other. If that were the case, it is straightforward to establish a damage coefficient D(E) for each proton energy relative to 10 MeV, then to multiply by a constant factor to convert 10 MeV protons to an equivalent number of 1 MeV electrons. One simply chooses a degradation level, 20% for example, and observes the fluences at 10 MeV, $\phi(10)$, and at energy E, $\phi(E)$, which produce a P_m/P_{mo} of 80% (throughout this report, we will define P_m/P_{mo} to mean the ratio of maximum power after some radiation level to the maximum power before irradiation). The damage coefficient for energy E, D(E), is given by the ratio $\phi(10)/\phi(E)$. The reference energy for calculating relative proton coefficients has historically been 10 MeV. As shown in Figure 3, this is convenient because the degradation curve for 10 MeV protons is a straight line on the plot ($\approx$20% P_m loss per decade of fluence) and it parallels the 1 MeV electron degradation curve very nicely. The 1 MeV electron and 10 MeV proton curves illustrate an equivalence of 3500 1 MeV electrons per 10 MeV proton, as compared with the value of 3000 used in Reference 2 (from now on referred to as the Handbook).

It is apparent from Figure 3 that the low energy proton curves do not always parallel the 10 MeV curve, and the D(E) values derived for those energies will depend on the degradation level chosen for calculating the fluence ratios. The question is, are these deviations sufficient to cause abandonment of this technique? This question will be addressed by a major

portion of this report. It is interesting to note that the original architects of the equivalent fluence procedure were faced with the same problem, but they found that in the final analysis of calculating power degradations in realistic isotropic radiation environments, it made very little difference.

Figures 4 through 6 are plots of similar sets of curves for GaAs cells including I_{sc} and V_{oc}. Here the curves generally seem to run parallel to each other in a more satisfactory manner and so we might expect there to be much less dependence of computed D(E)s on fluence. The factor to convert 10 MeV protons to equivalent 1 MeV electrons is found from the curves to be 1000 for P_m, 400 for I_{sc} and 2000 for V_{oc}.

Silicon damage coefficients relative to 10 MeV protons were computed as outlined above and plotted in Figure 7. In the figure, we show the result of calculating the D(E)s for both 10 ohm-cm and 2 ohm-cm cells over a range of P_m/P_{mo} ratios, with the ranges depicted by the hatched areas. The top of this range, computed by using P_m/P_{mo} = 70%, is nearly twice as large as the bottom of the range, where P_m/P_{mo} = 90% was used. Figure 7 also illustrates that relative to 10 MeV protons, the 2 ohm-cm D(E)s are lower than 10 ohm-cm D(E)s and that they are both lower than the values quoted in the Handbook. This does not mean that 2 ohm-cm cells are more resistant to low energy protons than 10 ohm-cm cells. It merely means that the ratio of fluence (to 10 MeV) is different for the two resistivities. The points shown at 8.3 MeV and higher were obtained in a previous set of measurements using the cyclotron at the University of California at Davis and irradiating similar solar cells (4). In the region between 1 and 10 MeV, we have only obtained data at 3 MeV. Since the damage coefficient vs. energy curve has a maximum in that region, we will need to obtain more data there in order to estimate these

curves with any degree of accuracy. In addition, protons with energies in this region contribute significantly to the degradation of solar arrays in proton-dominated orbits, so it is important to have a detailed knowledge of the damage coefficient behavior in this region. Future work will concentrate on characterizing cells in this energy region, but for now we will rely mostly on the curves drawn in the Handbook and show individual data points taken from our current set of measurements.

The relationship between 2 and 10 ohm-cm cells is directly compared in the curves of Figures 8 through 10 depicting normalized short circuit current, open circuit voltage, and maximum power as a function of 10 MeV proton fluence. As expected, the 10 ohm-cm cells exhibit a superior radiation resistance. However, a note of caution must be inserted here since 2 ohm-cm cells normally have higher initial maximum power than 10 ohm-cm cells. In fact, in this series of experiments the particular group of 2 and 10 ohm-cm cells used exhibited a tendency to converge in terms of absolute maximum power at the higher fluences at both 3 and 10 MeV. These figures also show that for penetrating radiation (10 MeV protons have a range of 713 microns in Si), the cell damage is independent of the angle of proton incidence, in agreement with the assumptions used in the Handbook. Similar data for 10 ohm-cm cells irradiated with 1 MeV protons are shown in Figures 11 through 13. These data at 1 MeV are typical of all the irradiations performed in the energy range between 0.1 and 1 MeV showing that for silicon cells, omni irradiations always cause considerably less cell parameter loss than normally incident irradiation.

Curves similar to those of Figure 7 were produced for the cells irradiated with the omni fixture, and damage coefficients computed. The resulting damage coefficients for 10 ohm-cm solar cells (appropriate for cells without coverglasses) are shown in Figure 14. Shown for comparison in Figure 14 are

the 10 ohm-cm normal incidence damage coefficients as well as the normal incidence and omni damage coefficients used in the Handbook. Both sets of experimental damage coefficients resulting from the present measurements below 1 MeV are shown as bands in this figure. These bands encompass the range of damage coefficient values as the reference level of P_m/P_{mo} is allowed to vary from 10% to 30% degradation (90% to 70% P_m/P_{mo}). Since the Handbook coefficients shown are derived for the case of infinite backshielding, the experimental values for the omnidirectional cases were derived by using half the fluences measured with the stationary Faraday cup. These curves suggest that the present experimental data are about the same amount below the comparable Handbook curves, so the technique used in the Handbook to compute the omni curves seems to work well. The data points at 3 MeV support the evidence that the Handbook values may be a little too high, but further data has to be acquired to fully define the curve.

Considering now only the high range of the normal incidence damage coefficients for 10 ohm-cm cells, we compute the omnidirectional damage coefficients for solar cells protected with various thicknesses of coverglasses. This is done by using the procedure outlined in the Handbook. The isotropic radiation damage coefficient for a solar cell protected by a coverglass of thickness t and infinite shielding on the rear surface, D(E,t), is

$$D(E,t) = \frac{1}{4\pi} \int_0^{\pi/2} D(E_o,\theta) \cos\theta \, d\Omega \qquad (1)$$

where

E = particle energy incident on the coverglass

E_o = particle energy as it emerges from the coverglass and strikes the solar cell

$D(E_o, \theta)$ = damage coefficient for unidirectional radiation of energy E_o striking the solar cell at incidence angle θ

$d\Omega$ = unit solid angle = $2\pi \sin \theta \, d\theta$

$\cos \theta$ = projected unit solar cell area

There are two cases to consider in evaluating $D(E_o, \theta)$: one in which the proton penetrates the solar cell, and one in which the proton stops in the solar cell.

Case 1, when the proton has more than enough energy to penetrate the coverglass and the solar cell at incidence angle θ, is illustrated in Figure 15. Such a proton will have a pathlength sec θ times that of a proton of energy E_o entering at normal incidence and will therefore produce approximately sec θ times as many displacements. For the case of total penetration, then,

$$D(E_o, \theta) = D(E_o, 0) \sec \theta \qquad (2)$$

When equation 2 is substituted into equation 1, it is apparent that the omnidirectional damage coefficient is independent of proton incidence angle for penetrating radiation. This is confirmed by the 10 MeV proton data in Figures 8 through 10.

Case 2 arises when the proton stops in the solar cell (Figure 16). After penetrating the coverglass, it will have some pathlength r in the solar cell. Measured from the front surface of the solar cell, this endpoint occurs at a depth $d = r \cos \theta$. The procedure here is to compute what proton energy is

required to penetrate to depth d when the proton enters at normal incidence. Let this energy be E_n. E_n will necessarily be $\leq E_o$ and a proton of this energy will produce damage to the same depth as the slanting proton of energy E_o. The slanting proton will produce an absolute number of displacements which is greater than the proton of energy E_n, so a correction factor is computed to compensate for this. The factor used is the ratio of total number of displacements produced by a proton of energy E_o, $N_d(E_o)$ to the total number of displacements produced by a proton of energy E_n, $N_d(E_n)$. We use the Kinchin and Pease model (5) for computing these displacement numbers.

The damage coefficient for a proton of energy E_o as it strikes the solar cell at incidence angle θ is therefore given by

$$D(E_o,\theta) = \frac{N_d(E_o)}{N_d(E_n)} D(E_n,0) \tag{3}$$

The calculation of D(E,t) may be summarized by

$$D(E,t) = \frac{1}{4\pi} \int_0^{\theta_p} D(E_o,0)\ 2\pi \sin\theta\, d\theta$$

$$+ \frac{1}{4\pi} \int_{\theta_p}^{\pi/2} D(E_n,0) \frac{N_d(E_o)}{N_d(E_n)}\ 2\pi \sin\theta \cos\theta\, d\theta \tag{4}$$

where θ_p is the incidence angle at which a proton of energy E will just penetrate both the coverglass and the solar cell.

An integration of equation 4 is done numerically by computer using the present proton degradation data to produce the family of curves shown in Figure 17. Each curve is produced for the particular coverglass thickness shown. Also shown in Figure 17 is the normal incidence damage coefficient curve from which the others are derived. This curve is shown as a dashed line

at energies higher than 1 MeV, where our new data base is lacking. This dashed curve represents our effort to mate the present data with the curve used in the Handbook. We have also plotted some experimental points on Figure 17 which were derived from the omnidirectional irradiations. The agreement with the calculation is quite good.

In order to further compare the computed omni D(E)s with experiment, we computed the degradation of a solar cell irradiated with 300 keV omni protons, and compared this with our experimental results. The proton fluence was multiplied by the appropriate omni damage coefficient taken from Figure 17 to convert to equivalent 10 MeV protons, then multiplied by 3500 to convert to equivalent 1 MeV electrons. The appropriate P_m/P_{mo} degradation curve vs 1 MeV electron fluence in the Handbook was then used to compute remaining power. The result of this computation is shown in Figure 18. The experimental and omni curves from our present experiments are shown for comparison. The computed equivalent 1 MeV electron fluences were multiplied by 2 because the calculations assume infinite backshielding, but the experimental setup causes the radiation that would usually be incident on the rear 2π steradians of cell surface to fall instead on the front 2π steradians. Figure 18 shows that the Handbook procedure in this case overestimates the amount of solar cell degradation up until the degradation reaches a P_m/P_{mo} of 70%. However, the deviation between experiment and calculation is less than 4%.

Figures 19 and 20 depict degradation curves of VJ and BSF solar cells as a function of proton fluence in comparison with the non-field 10 ohm-cm cells. The grooves of the VJ cells were aligned parallel to the rotation axis of the omnidirectional rotation fixture during the irradiations. Figure 19 shows that the power output of the VJ cells remained higher than that of the 10 ohm-cm cells throughout the fluence range tested. In Figure 20, BSF cells are com-

pared with otherwise identical 10 ohm-cm cells at 1.0 and 10 MeV. In each case the BSF cells start out with higher absolute power. As the exposure increases, however, the P_m of the two cell types tend to converge. This is apparently caused by a removal of the field effectiveness by relatively low proton fluences, followed by a decrease in power caused by minority carrier diffusion length degradation. Since this loss of minority carrier diffusion length occurs equally in both field and non-field cells, the two types degrade similarly once the field effectiveness is removed.

The same type of normal incidence and omnidirectional irradiations were carried out for the p/n LPE GaAs solar cells. Ten-ohm-cm silicon control cells were included with each GaAs cell run and their degradation behavior was constantly checked for consistency with the appropriate silicon runs. The data for each of the seven energies used are summarized in Tables A-1 through A-7 in the Appendix. Some typical degradation curves are shown in Figures 21 through 29 for proton energies of 0.05, 1.0 and 10 MeV protons, respectively. Although the 50 keV protons should stop in the GaAlAs window, they produce a considerable amount of degradation in the solar cell output at normal incidence. Since HRL specifies window thicknesses to be $X_w \leq 0.5$ microns, it is possible that the windows are in fact thin enough to allow proton penetration to the junction and would reasonably explain the observed degradation. Unlike degradation of silicon cells which do not lose I_{sc} under low energy proton irradiation, the GaAs cells lost 30% of their initial I_{sc}, 10% of their initial V_{oc} and reached approximately a 40% loss in P_m as a result of the 50 keV bombardment. Figures 24 through 26 show the interesting phenomena of the 1.0 MeV omni fluence causing greater degradation than the normal incidence fluence. This was not observed for any proton energy in the silicon cell experiments. It is thought to be caused by slant range protons

coming to rest in the junction area. Since protons produce most of their damage at the end-of-track, these protons are likely to cause much more serious damage than they would at normal incidence when the end-of-track would terminate in a less sensitive part of the cell. Figure 29 shows the P_m curves for the 10 MeV irradiations. Surprisingly, here, too, the omni irradiation degrades the cell more than the normal incidence radiation, although the difference is slight (≈2%). These data raise a serious question about the validity of performing spectra testing of GaAs cells using normal incidence irradiations. In spectra irradiations, the fluence-energy spectrum of a particular flight orbit of interest is broken up into a discrete set of energy intervals, then the test solar cells are irradiated to appropriate fluence levels in each energy interval. These results strongly suggest that this procedure should be carried out with an omni simulation fixture to avoid underestimating the damage.

The procedures outlined above for silicon were carried out in the analysis of the GaAs data. The normal incidence damage coefficients for P_m relative to 10 MeV protons are shown in Figure 30, in comparison with the silicon damage coefficients from the Handbook. The most striking feature about this curve is the large values of the GaAs coefficients between 50 keV and 1 MeV. The GaAs damage coefficients are a factor of 30 higher than for silicon at 150 keV. As for Si, we also find a range of damage coefficients, which are bounded by the lines labeled "high" and "low" in the figure. The dashed lines indicate those areas where we had little data but interpolated between the low and high energy data. We did, however, consult the proton radiation data reported by Loo et al. (6) taken at 2, 5, and 10 MeV to derive coefficients for 2 and 5 MeV. These values were found to agree very closely with the interpolation used. The coefficients for energies higher than 10 MeV were again computed from the work of Reference 4. In Reference 7 we showed that

the difference in the damage coefficients at low proton energies did not affect the orbital calculations when coverglasses of 1 mil or more are employed. We have recently acquired data at 3 MeV for GaAs solar cells and the computed 3 MeV damage coefficient is plotted in the figure. This data point is also consistent with the interpolation used. For GaAs, the damage coefficient maxima occur in the 100 to 200 keV range. The maxima and low energy rolloff are well defined in the experimental results presented in this report. In the range of 200 keV to 10 MeV, GaAs damage coefficents appear to exhibit an approximate 1/E dependence on proton energy as exhibited by the data at 0.5, 1, 3, and 10 MeV, contrary to the situation for silicon solar cells. For these reasons, we feel that the mean damage coefficient curves for GaAs cells presented here are more accurate than the curves for silicon cells for the energies covered so far. Using the routines given in the Handbook, omni calculations as a function of coverglass thickness for short circuit current, open circuit voltage, and maximum power were performed as shown in Figures 31 through 33. Also shown in these figures are the experimental data acquired for zero coverglass thickness from the omni irradiations. The agreement between computed and measured omni data indicates that this procedure is working as well for GaAs as it did for silicon.

A calculation was made to estimate how these cells would perform in some proton-dominated orbits. Three circular orbits were chosen: 1000 nautical miles (nmi) altitude, 0^{o} inclination; 3000 nmi, 0^{o} inclination; and 5600 nmi, 63^{o} inclination. The integral spectra of each orbit, derived from the AP8 trapped radiation models (8), are shown in Figures 34 and 35. The 1000 nmi spectrum contains almost all high energy protons (E>8 MeV), while the 3000 nmi spectrum has a large number of protons of all energies. Solar cell degradations were computed for each of these orbits for Si and GaAs cells.

Three sets of damage coefficients were used for each spectrum for the Si calculations (Handbook values, high range from the present data, and low range from the present data). Figure 36 is a plot of P_m/P_{mo} for 10 ohm-cm silicon cells vs coverglass thickness for the 1000 nmi and the 3000 nmi proton environments and for each set of damage coefficients. There is very little difference in the calculation no matter which set of coefficients is used, even though the difference between the three sets appeared to be enormous in Figure 14. The values for the damage coefficients in the energy range from 1 to 100 MeV clearly dominate the calculation.

Similar computations were performed for GaAs using the three orbits previously described. The short circuit current, open circuit voltage, and maximum power normal damage coefficients, shown in Figures 31 through 33, were used. The results for each orbit are shown in Figures 37 through 39. In each figure are shown normalized short circuit current, open circuit voltage, and maximum power. Examination of the damage coefficient data in Figures 31 through 33 reveals that the individual cell parameter coefficients are very similar, especially at energies above 1 MeV. Therefore a new set of I_{sc} and V_{oc} computations was performed for all three cell parameters in all three orbits using only the maximum power damage coefficients and the appropriate factors for conversion to equivalent 1 MeV electrons. The results of this simplified calculation were compared with the data of Figures 37 through 39. The comparison showed that there is less than a 1% difference between using the maximum power damage coefficient for short circuit current and open circuit voltage calculations, or using each individual damage coefficient for its related cell parameter for all three orbits and all glass thicknesses of 1 mil or more. Since orbital predictions have uncertainties far in excess of

1%, it seems feasible to use the GaAs maximum power damage coefficient for computation of all three cell parameters of interest.

In Figures 40 and 41, we plot absolute P_m vs coverglass thickness for GaAs and compare it with the calculations for Si cells. Similarly, in Figure 42 we plot absolute P_m vs. time in orbit at 5600 nmi for a 12 mil coverglass. It is evident that the considerably higher damage coefficients for GaAs in the low energy proton range do not play a significant role in orbit calculations when coverglasses are used. These curves would seem to indicate that GaAs solar cells should be an advantageous choice in some orbits.

SECTION IV

CONCLUSIONS

The conclusions that may be drawn from this study can be summarized as follows:

(1) The present data indicate that the equivalent fluence concept is an adequate method of predicting solar panel performance in space radiation environments. The damage coefficients for P_m reported in the Solar Cell Radiation Handbook are in substantial agreement with the present work, but they do need some minor modifications.

(2) The equivalent fluence concept appears to work well for GaAs solar cells. In addition, the energy dependence of the damage coefficient appears to be well established, with the possible exception of further device developments which may change the situation described above.

(3) Based on a preliminary calculation, using interpolations in the mid-energy range of the proton data, GaAs solar cells appear to perform well in proton-dominated environments.

REFERENCES

1. J. R. Carter, Jr., and H. Y. Tada, Solar Cell Radiation Handbook, Doc. No. 21945-6001-RU-00, TRW Systems Group, Redondo Beach, California, June 28, 1973, prepared under JPL Contract No. 953362.

2. H. Y. Tada, J. R. Carter, Jr., B. E. Anspaugh, and R. G. Downing, Solar Cell Radiation Handbook, JPL Publication 82-69, Jet Propulsion Laboratory, Pasadena, California, Nov. 1982.

3. J. Bernard, S. Mottet, and D. Sarrail, "Protons Isotropic Irradiation of Solar Cells," Conf. Rec. of the 12th IEEE Photovoltaic Specialists Conf., 216, 1976.

4. B. E. Anspaugh and R. G. Downing, "Damage Coefficients and Thermal Annealing of Irradiated Silicon and GaAs Solar Cells," Conf. Rec. of the 15th IEEE Photovoltaic Specialists Conf., 499, 1981.

5. G. H. Kinchin and R. S. Pease, "The Displacement of Atoms in Solids by Radiation," Report Prog. Physics 18, 1, 1955.

6. R. Y. Loo, G. S. Kamath, and R. C. Knechtli, Medium Energy Proton Radiation Damage to (AlGa)As-GaAs Solar Cells, NASA Contractor Report NASA-CR-165946, 1982.

7. B. E. Anspaugh and R. G. Downing, "Radiation Effects in Silicon and Gallium Arsenide Solar Cells Using Isotropic and Normally Incident Radiation," Conf. Rec. of the 17th IEEE Photovoltaic Specialists Conf., to be published.

8. D. M. Sawyer and J. I. Vette, AP8 Trapped Proton Environment for Solar Maximum and Solar Minimum, NSSDC/WDC-A-R&S 76-06, National Space Science Data Center, Goddard Space Flight Center, Greenbelt, Maryland, 1976.

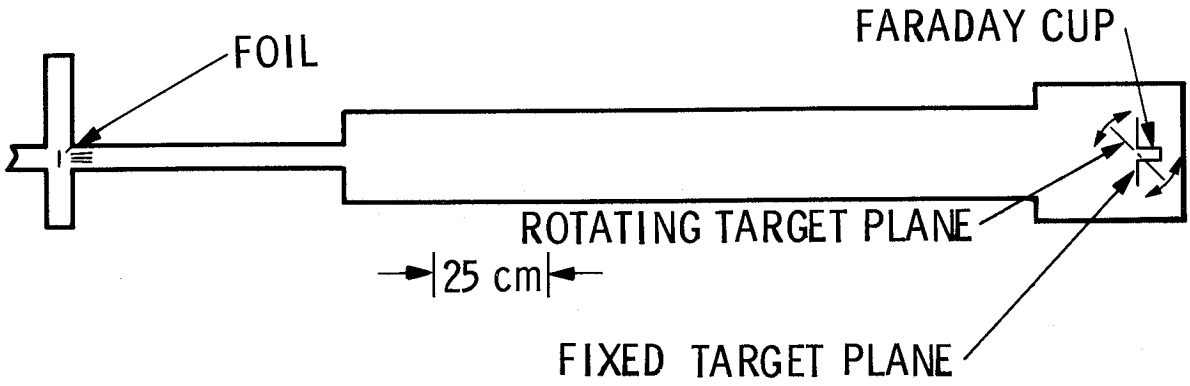

Figure 1. Schematic of Proton Irradiation Chamber

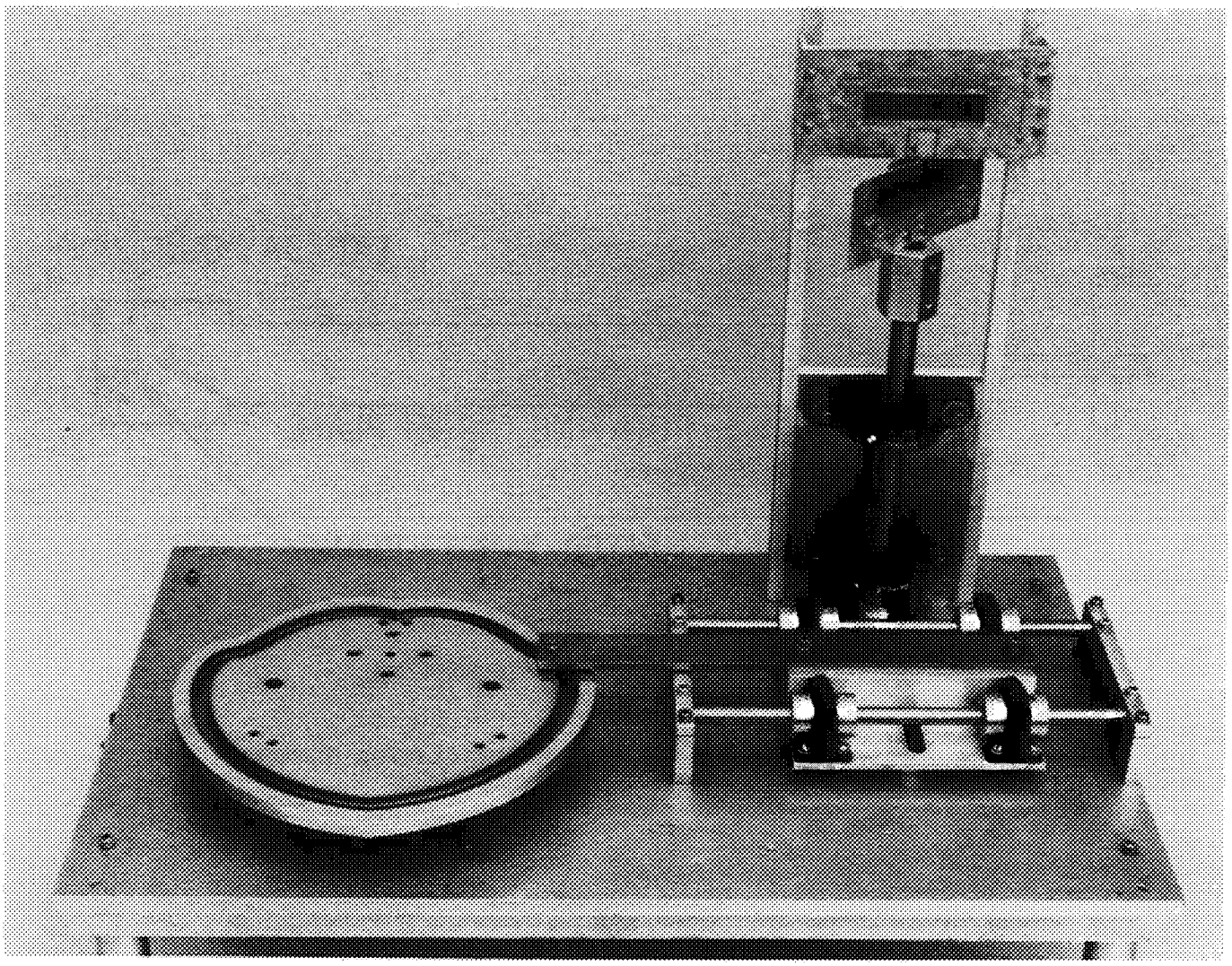

Figure 2. Cam Mechanism for Producing Simulated Omnidirectional Isotropic Irradiations

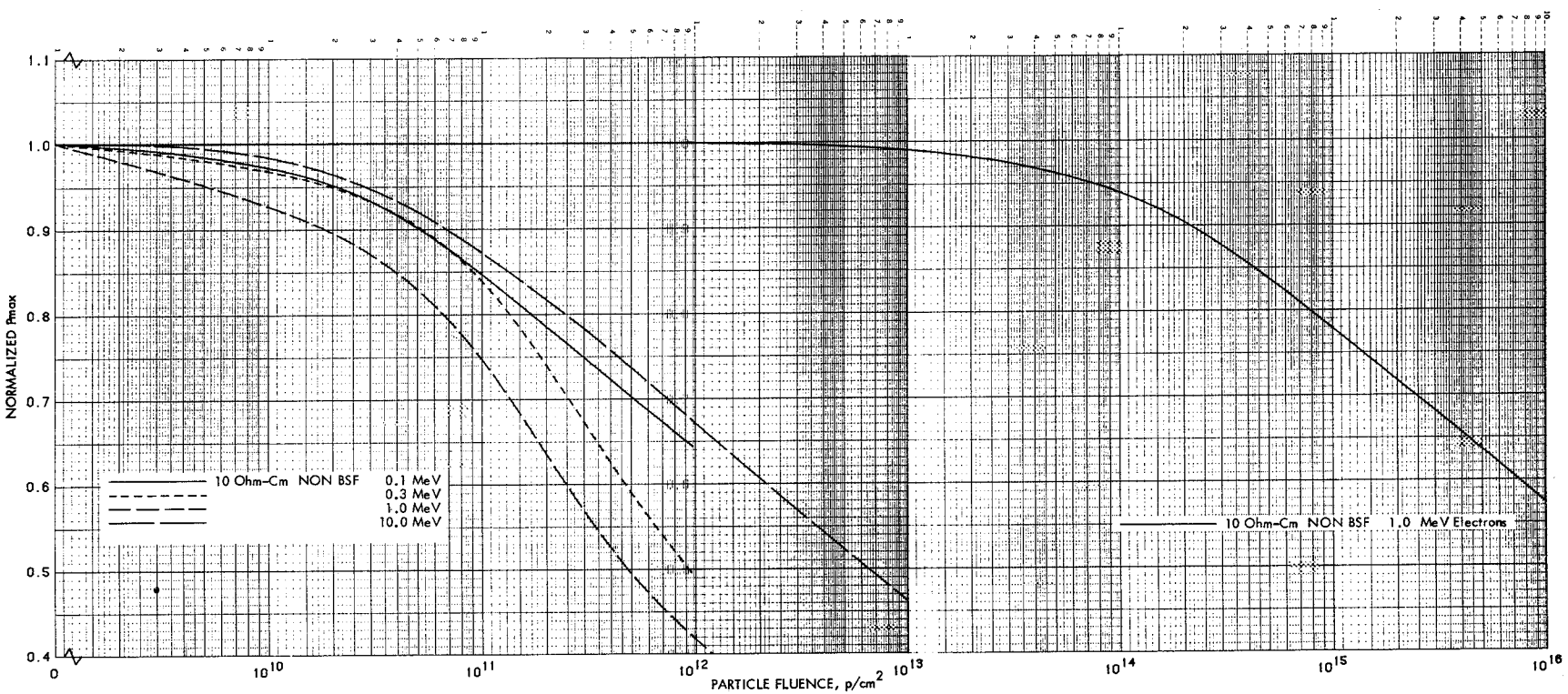

Figure 3. Particle and Energy Dependence of Silicon P_m Degradation

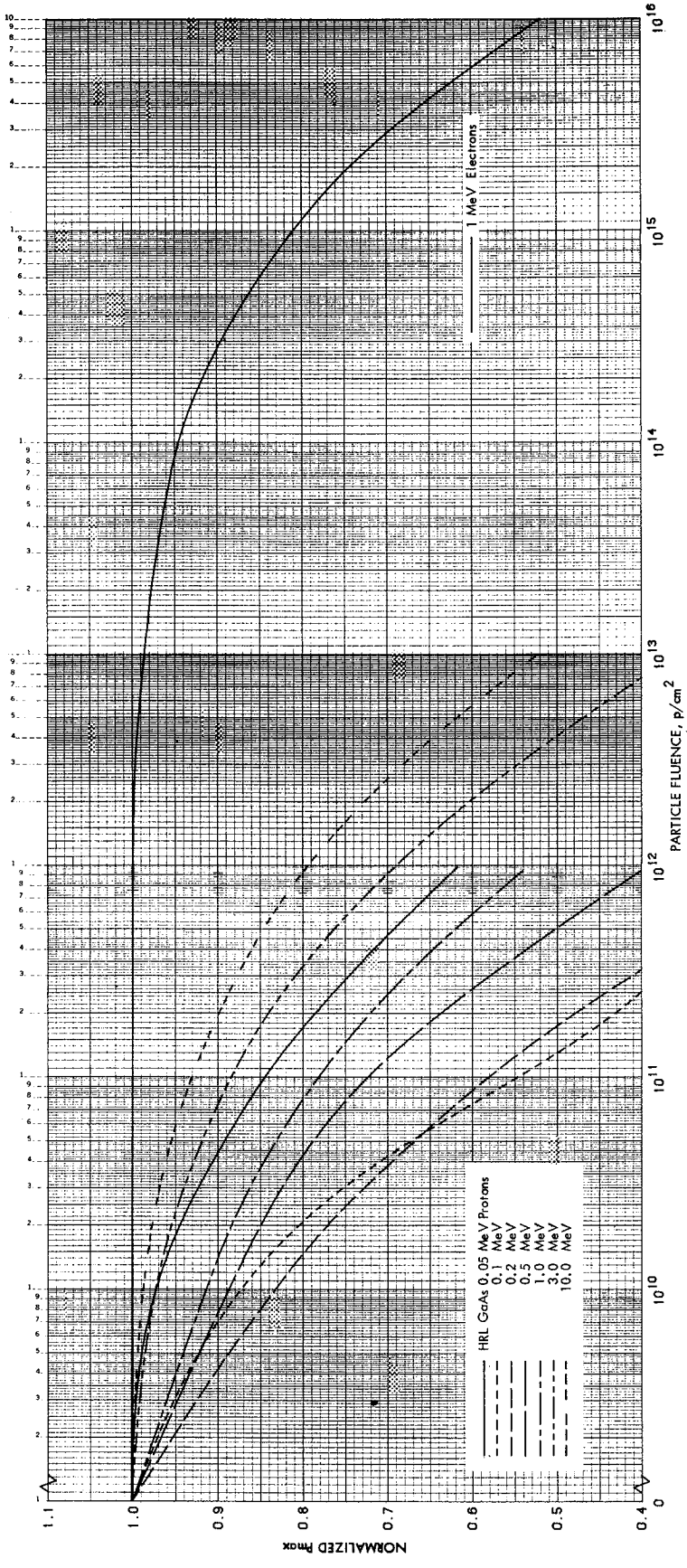

Figure 4. Particle and Energy Dependence of GaAs P_m Degradation

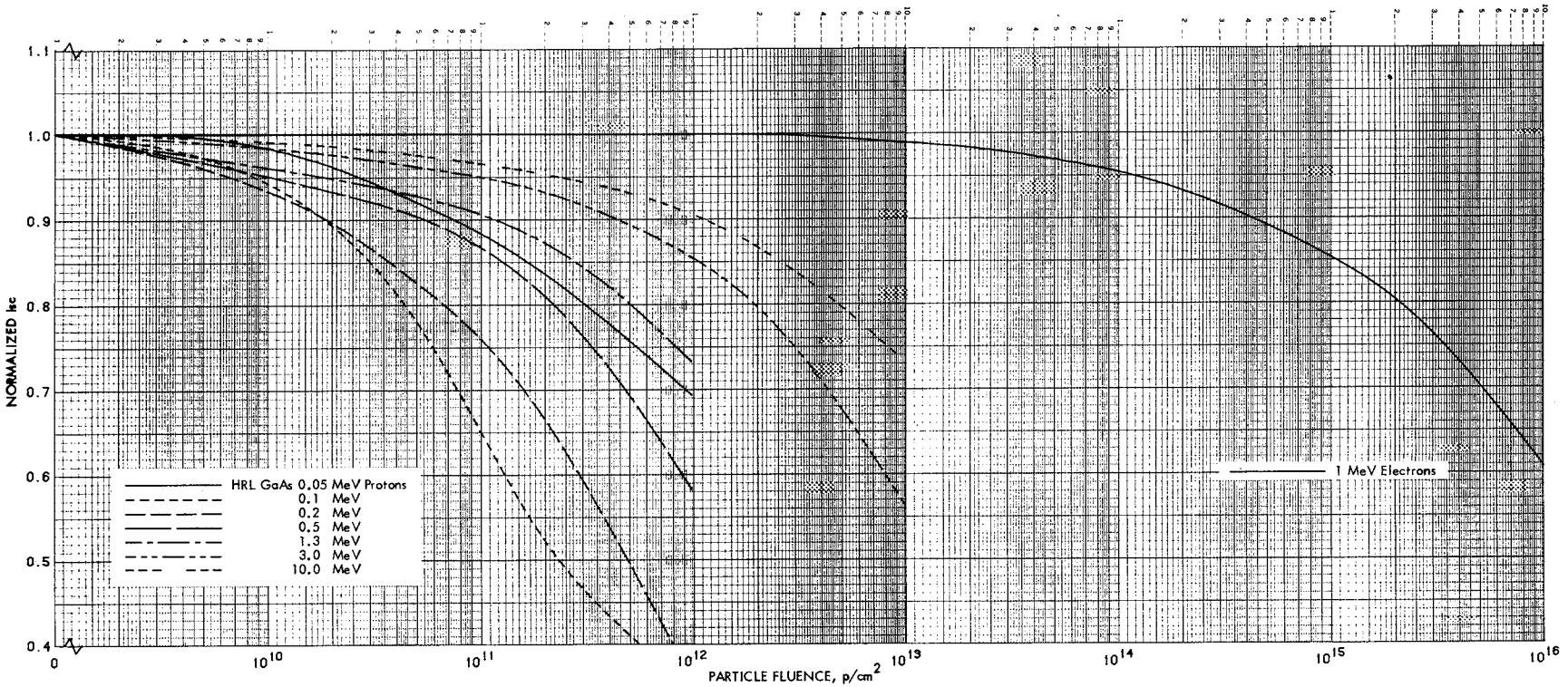

Figure 5. Particle and Energy Dependence of GaAs I_{sc} Degradation

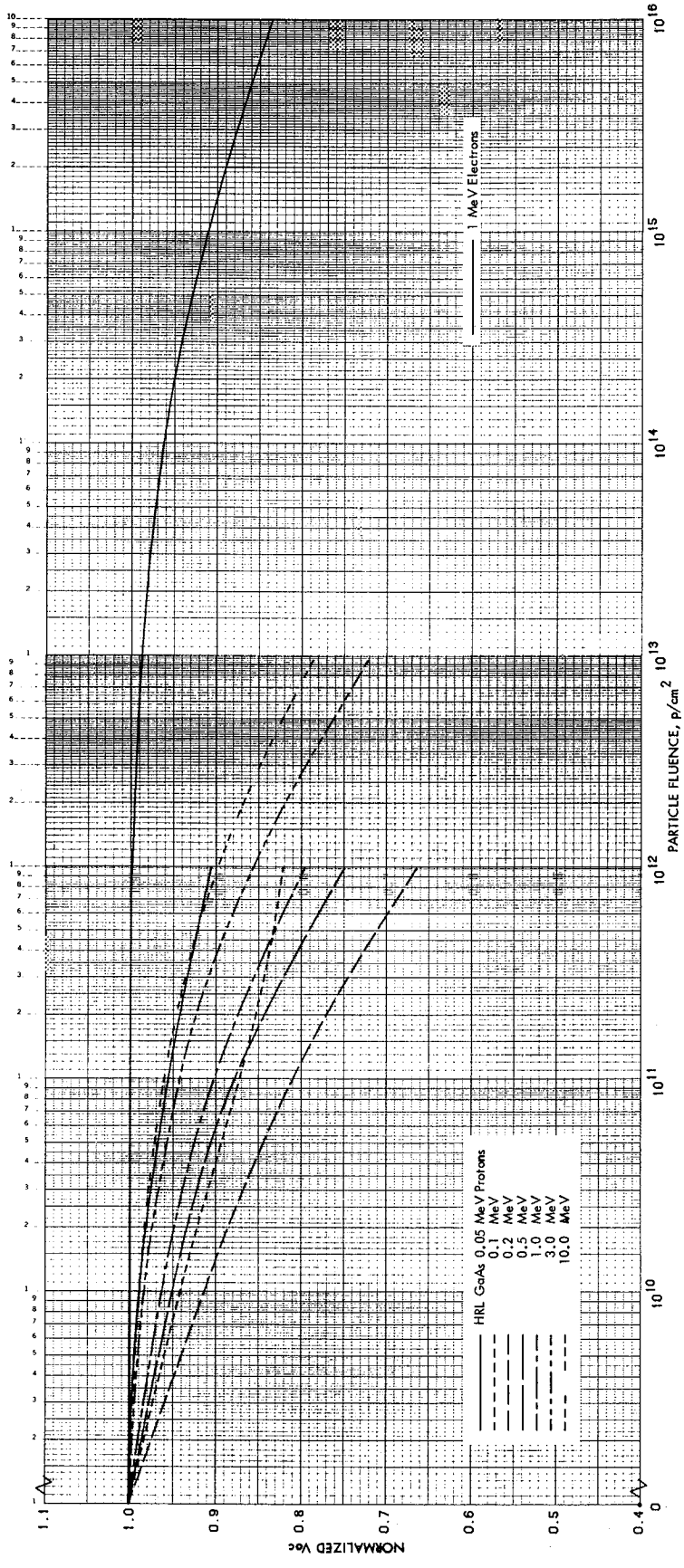

Figure 6. Particle and Energy Dependence of GaAs V_{oc} Degradation

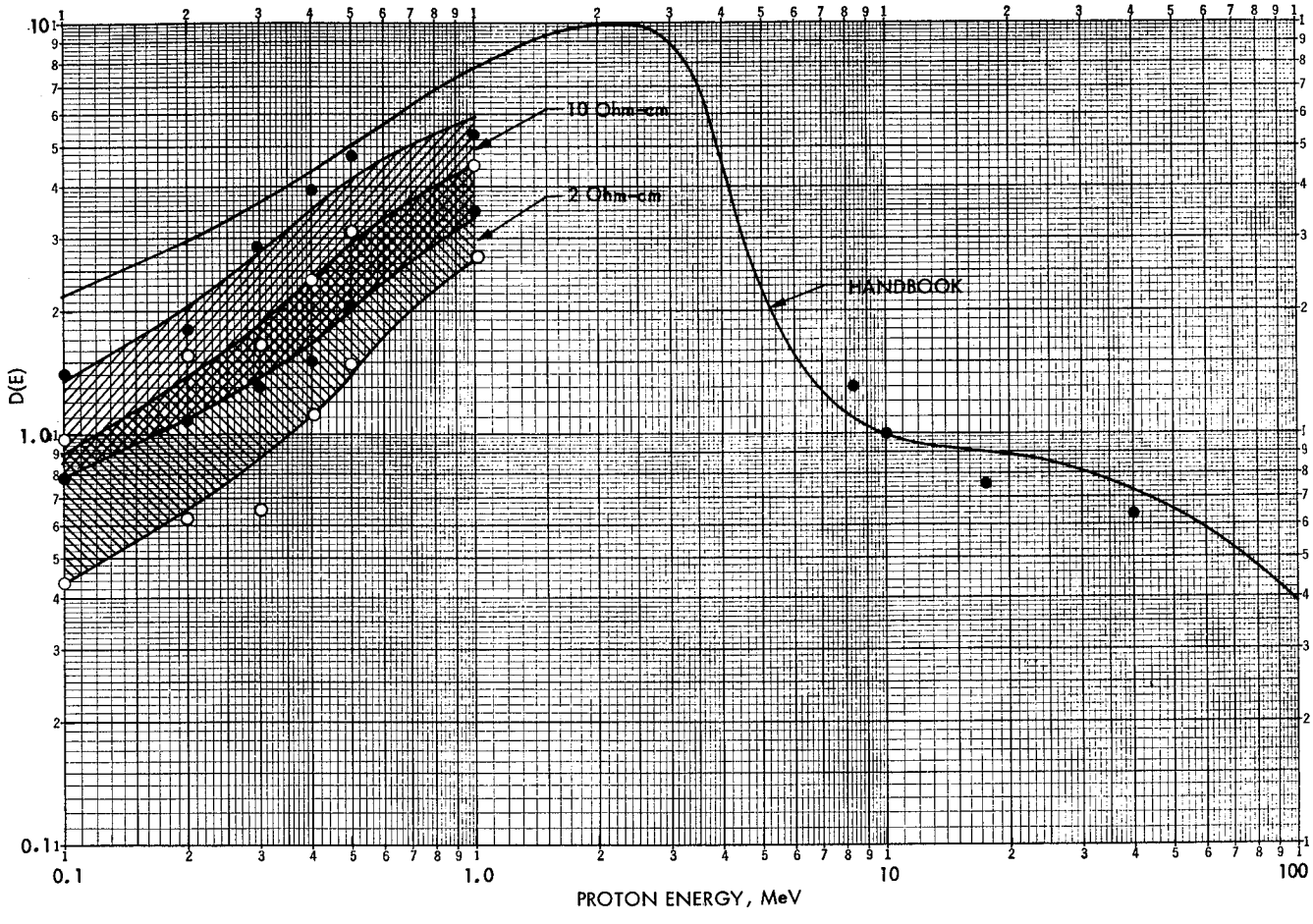

Figure 7. P_m Normal Incidence Damage Coefficients for Silicon Solar Cells

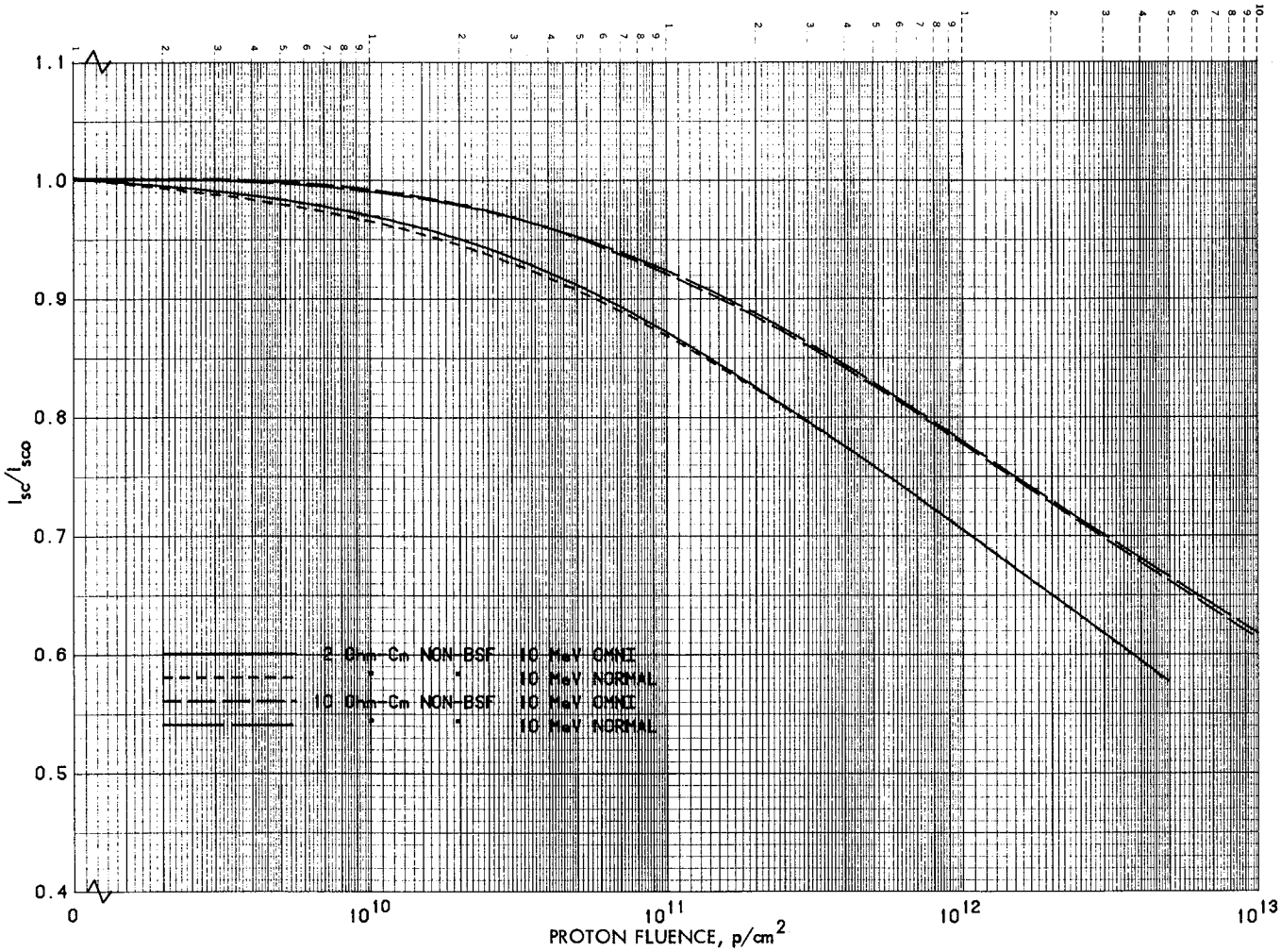

Figure 8. I_{sc} Degradation vs Omni and Normal Incidence, 10 MeV Proton Fluence

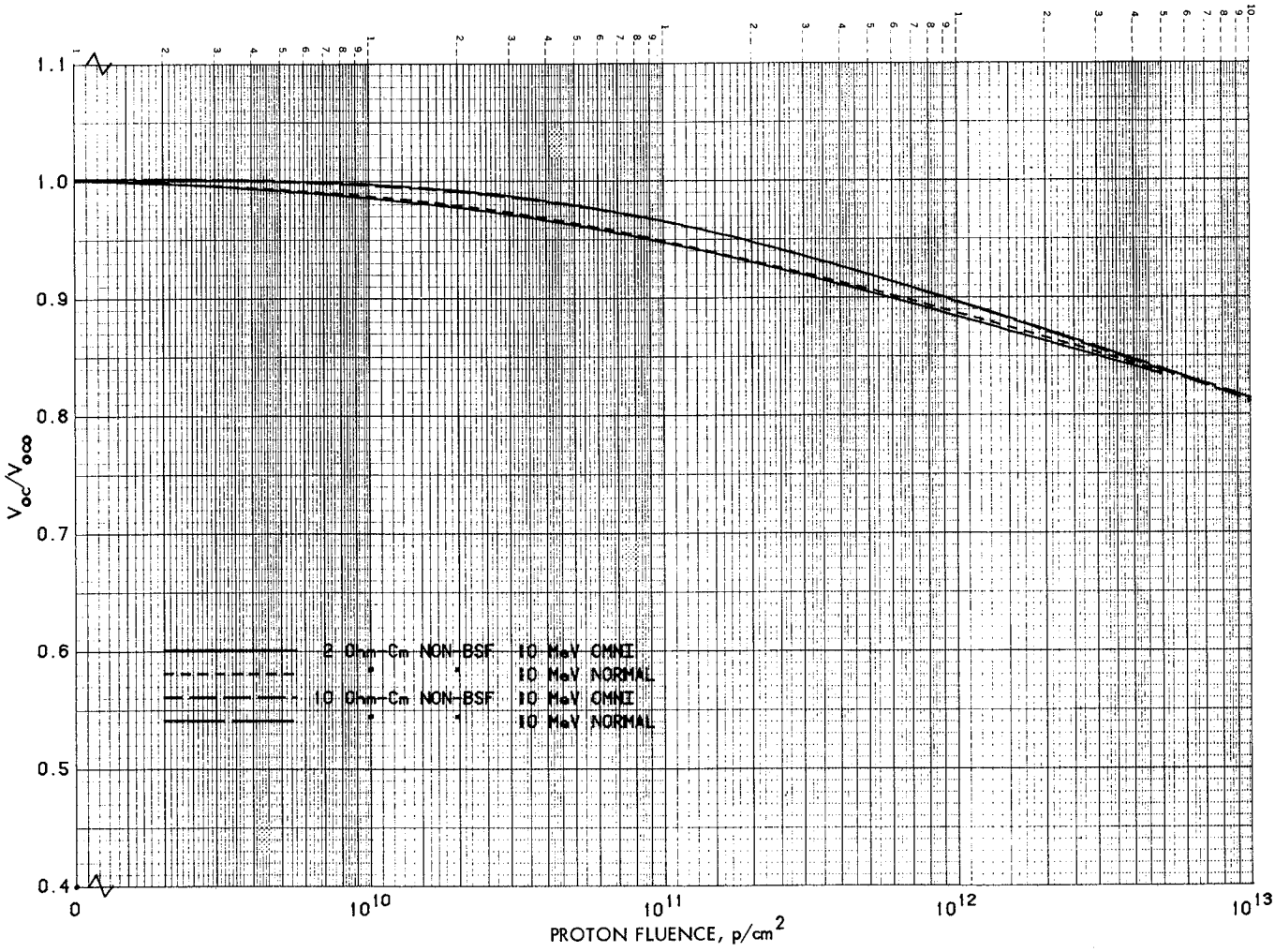

Figure 9. V_{oc} Degradation vs Omni and Normal Incidence, 10 MeV Proton Fluence

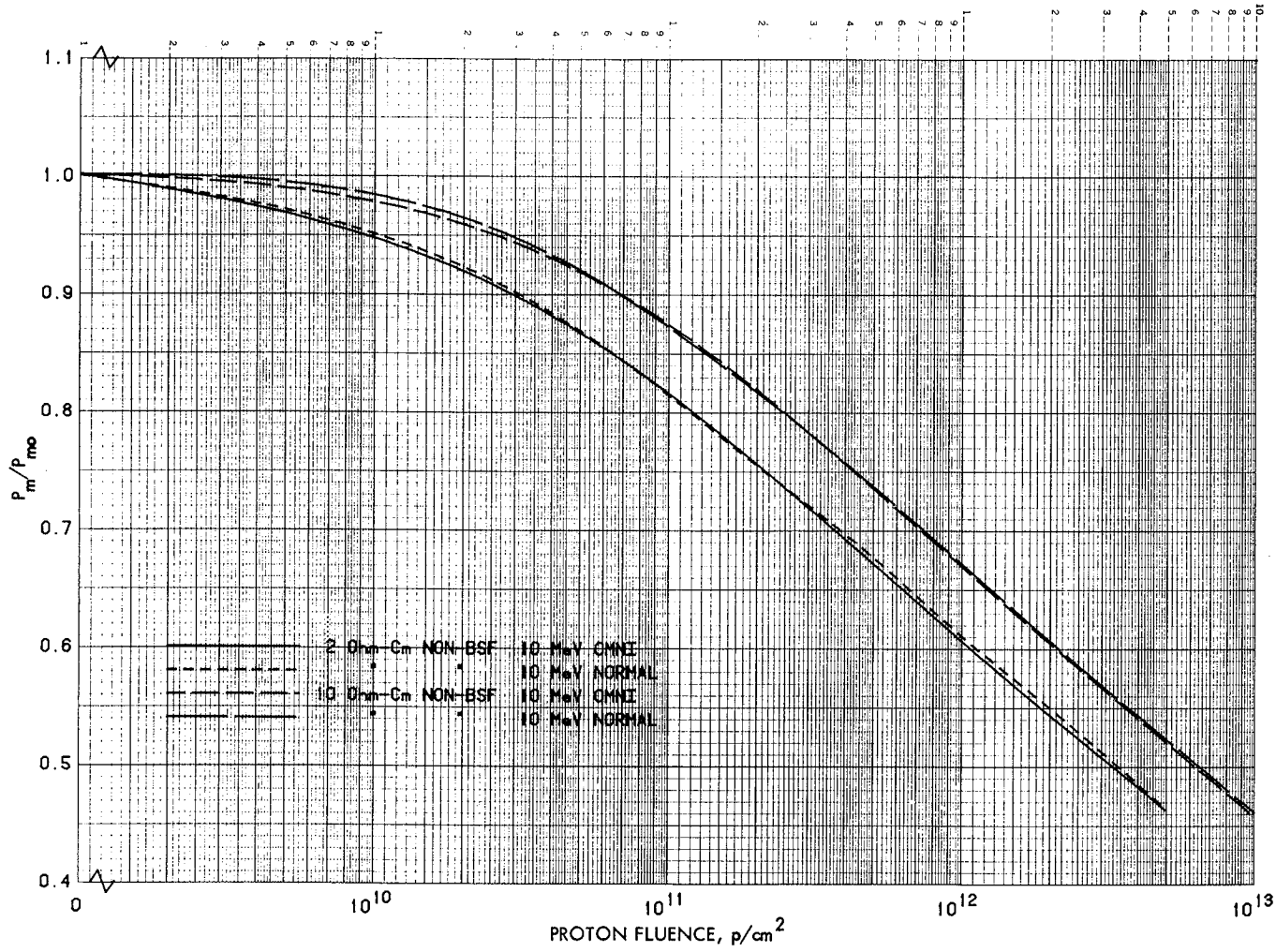

Figure 10. P_m Degradation vs Omni and Normal Incidence, 10 MeV Proton Fluence

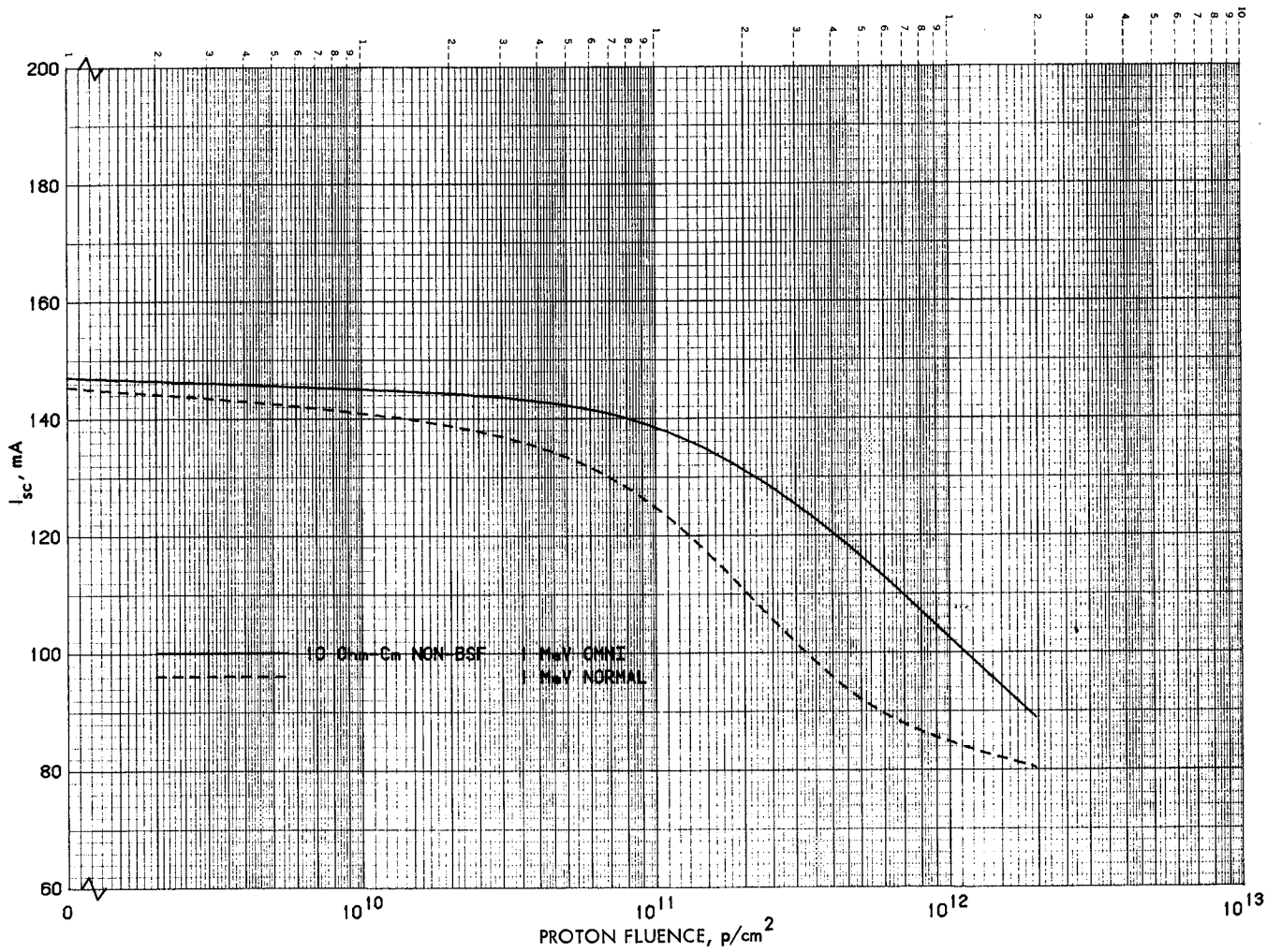

Figure 11. I_{sc} Degradation vs Omni and Normal Incidence, 1 MeV Proton Fluence

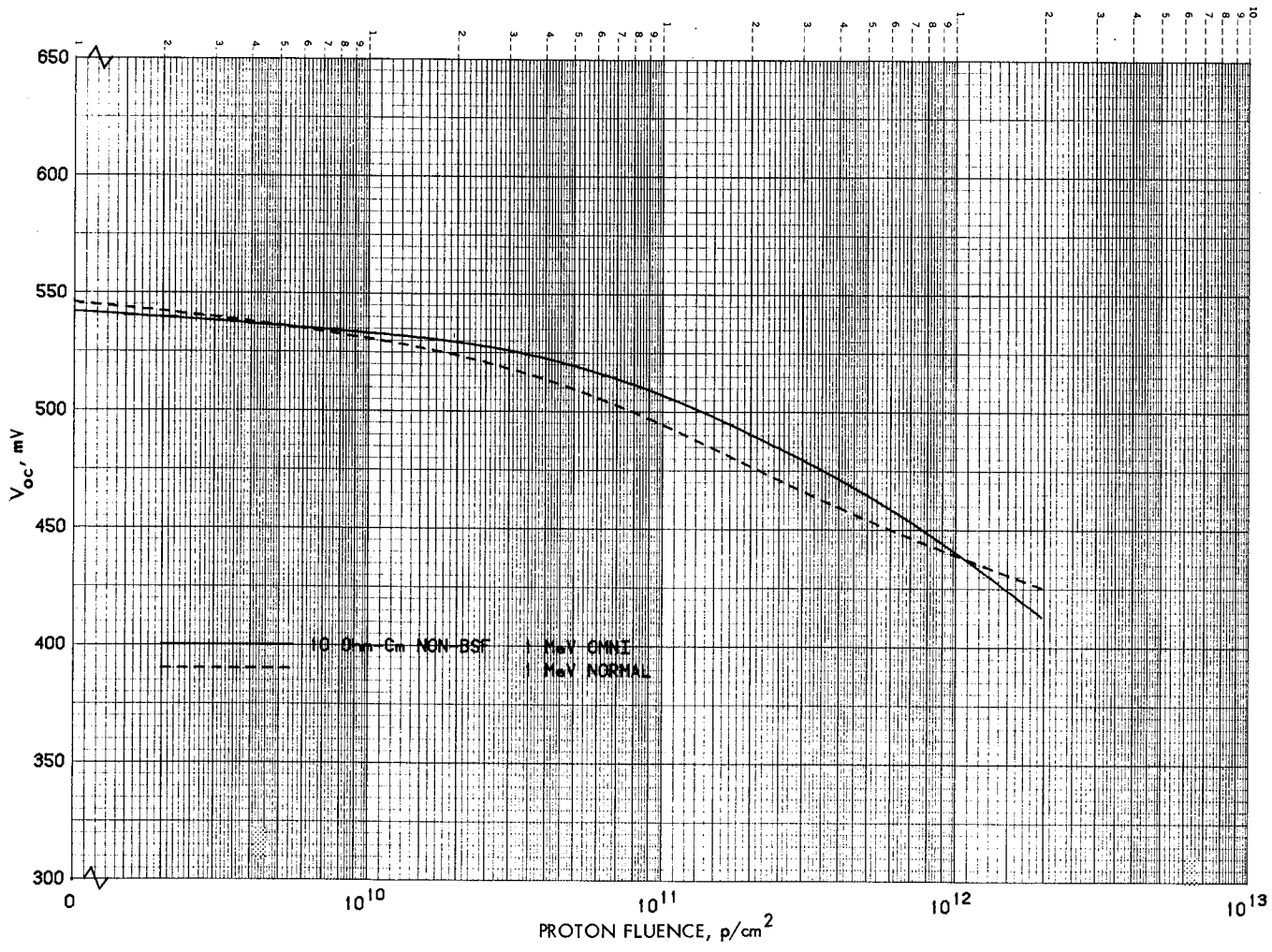

Figure 12. V_{oc} Degradation vs Omni and Normal Incidence, 1 MeV Proton Fluence

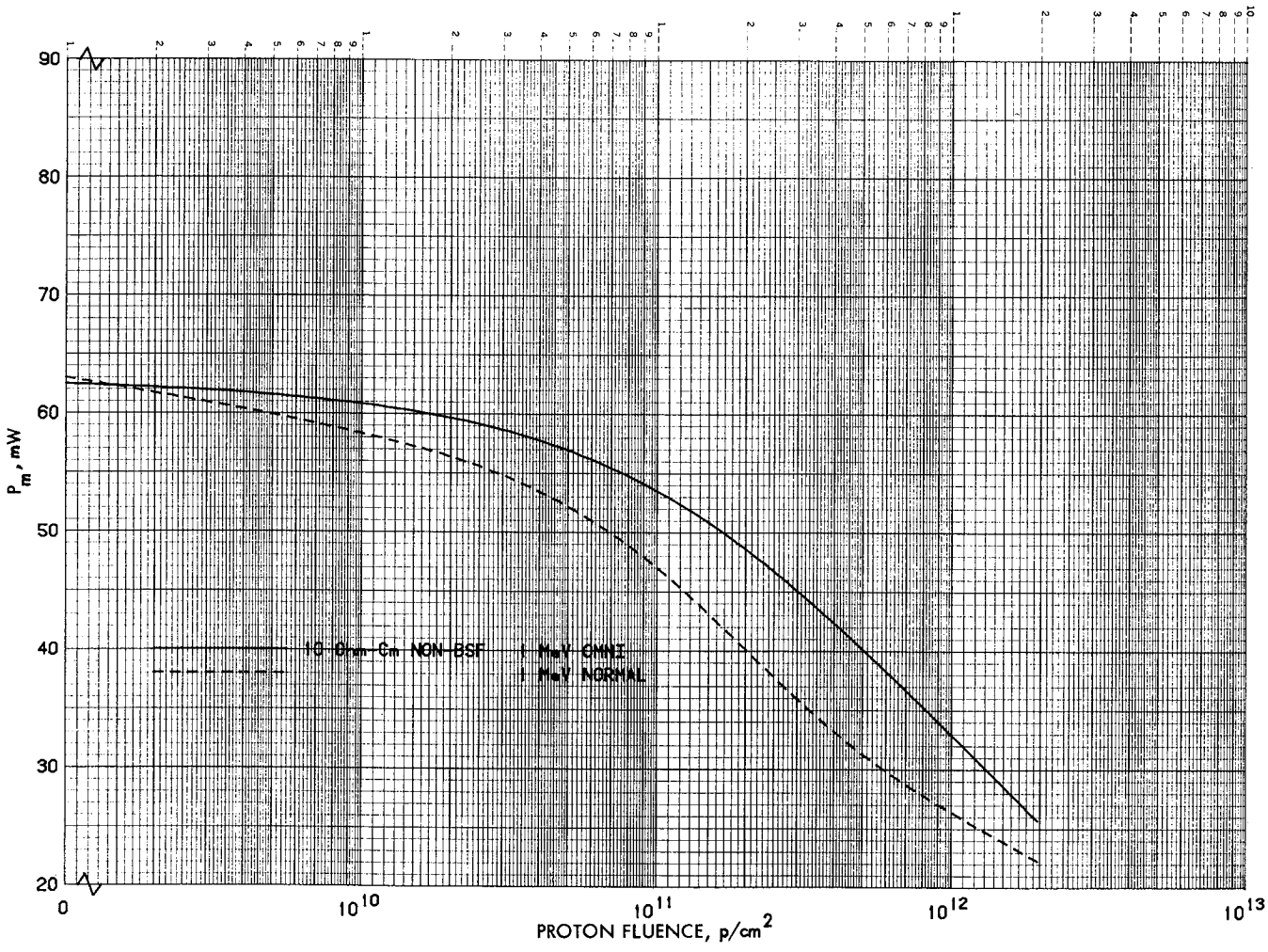

Figure 13. P_m Degradation vs Omni and Normal Incidence, 1 MeV Proton Fluence

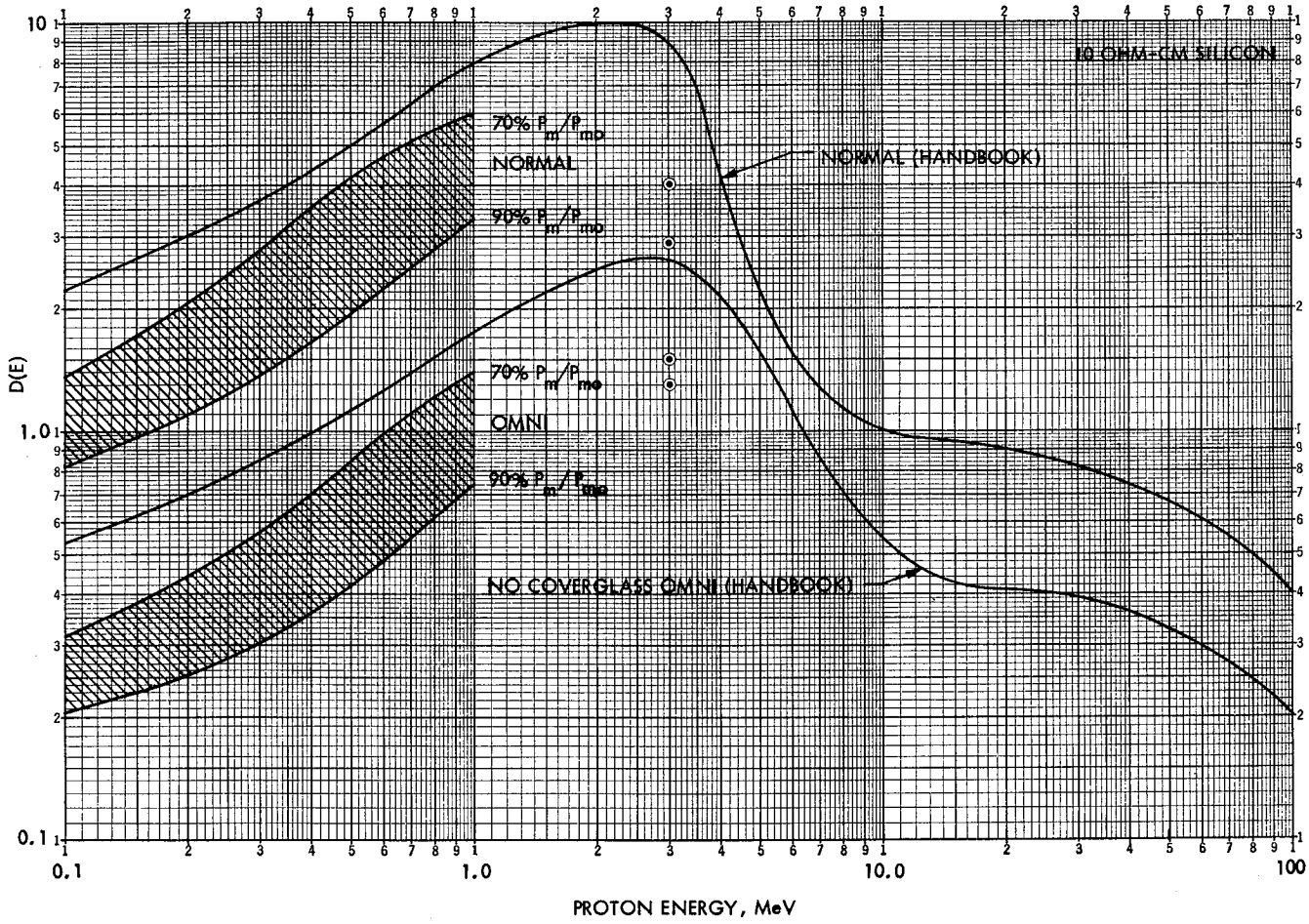

Figure 14. Comparison of Handbook P_m Damage Coefficients with Experiment

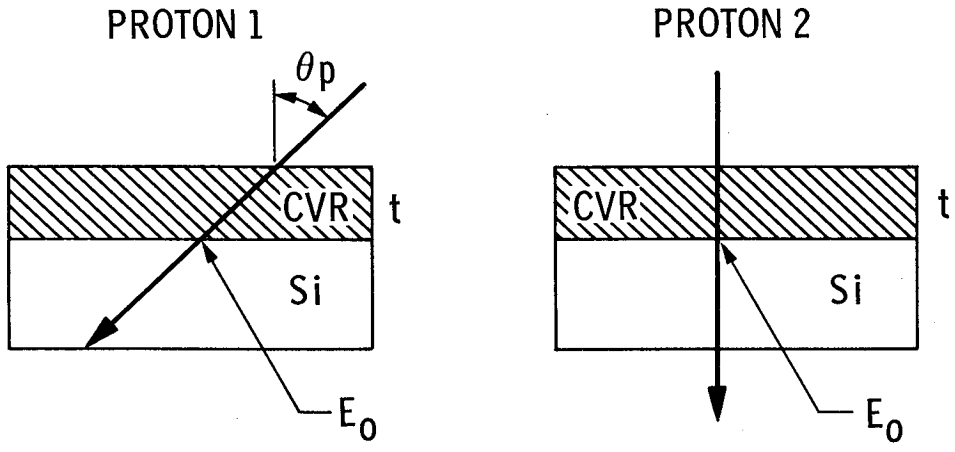

1. PROTON 1 AND PROTON 2 EACH ENTER THE SOLAR CELL WITH ENERGY E_0
2. PROTON 1 HAS ENERGY E WHEN IT STRIKES THE COVERGLASS AT $\theta = \theta_p$. IT JUST PENETRATES COVERGLASS AND SOLAR CELL
3. PROTON 1 HAS A PATH LENGTH $\frac{1}{\cos\theta}$ TIMES THAT OF PROTON 2 AND PRODUCES MORE DISPLACEMENTS BY THE SAME FACTOR
4. $D(E_0, \theta) = \frac{D(E_0, 0)}{\cos\theta}$

Figure 15. Omnidirectional Damage Coefficient Calculation for Protons which Penetrate Coverglass and Solar Cell

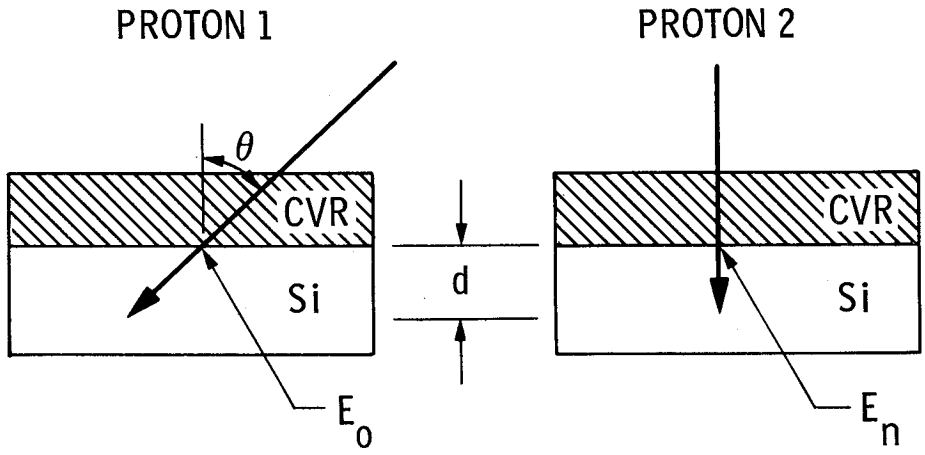

1. EACH PENETRATES TO SAME DEPTH, d, IN THE SOLAR CELL
2. PROTON 1 ENTERS CELL WITH ENERGY E_0, PRODUCES n_1 DEFECTS IN Si
   PROTON 2 ENTERS CELL WITH ENERGY E_n, PRODUCES n_2 DEFECTS IN Si
3. PROTON 1 PRODUCES MORE CELL DAMAGE THAN PROTON 2 BY FACTOR: $\frac{n_1}{n_2}$
4. $D(E_0, \theta) = \frac{n_1}{n_2} D(E_n, 0)$

Figure 16. Omnidirectional Damage Coefficient Calculation for Protons which Stop in the Solar Cell

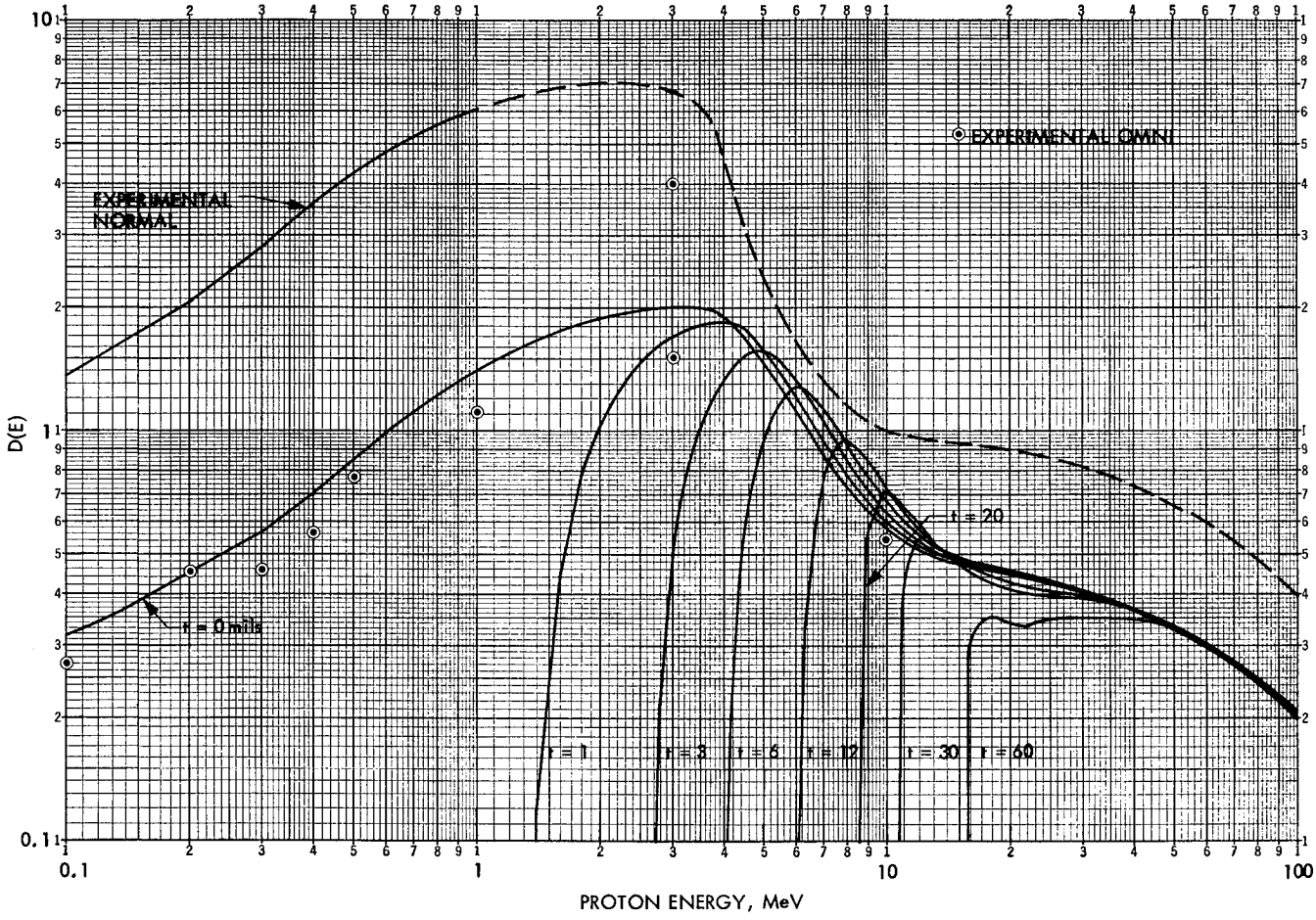

Figure 17. Experimental and Computed P_m Omnidirectional Damage Coefficients for Silicon Solar Cells

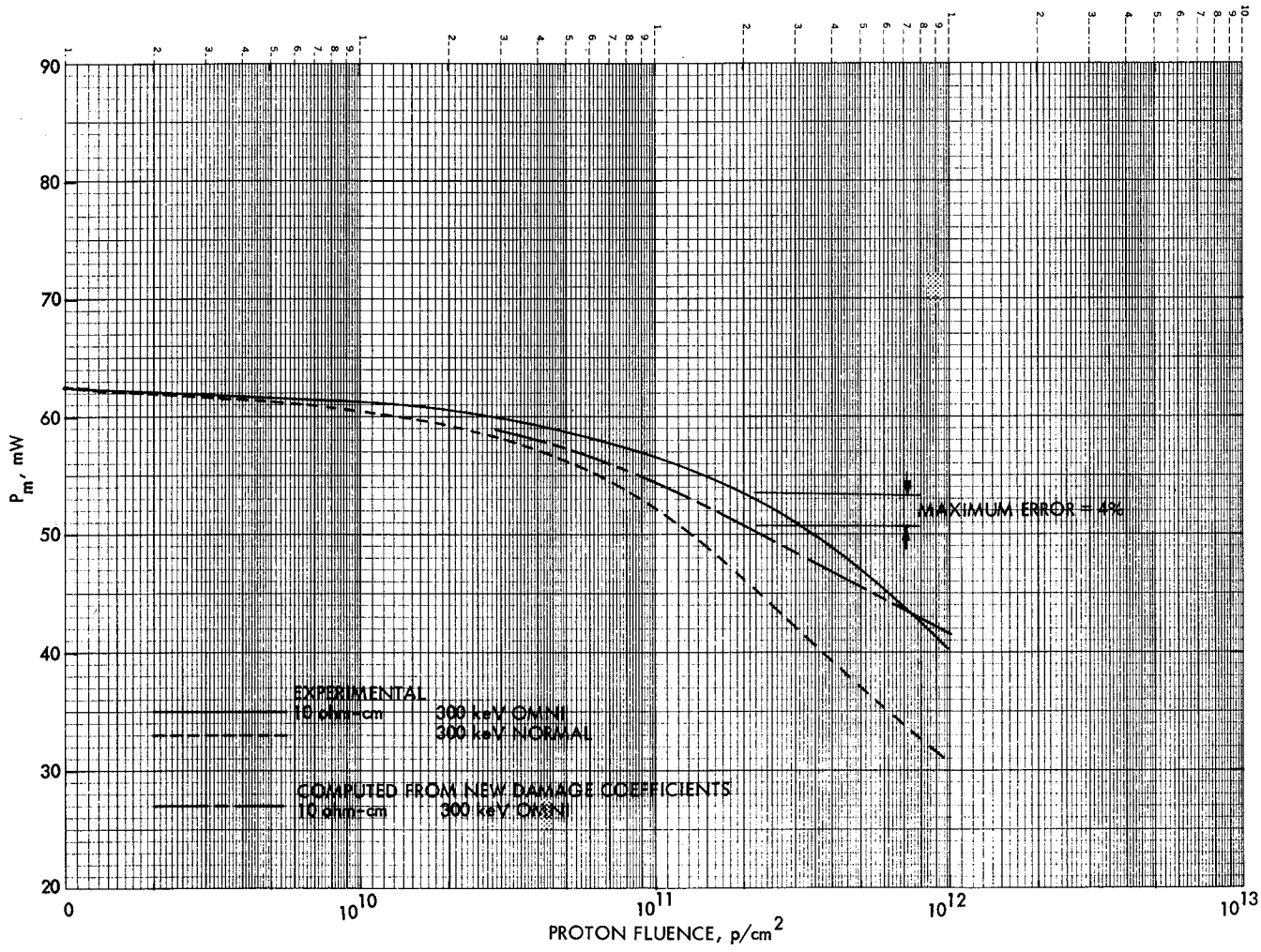

Figure 18. Experimental and Computed P_m Solar Cell Degradation by 300 keV Protons

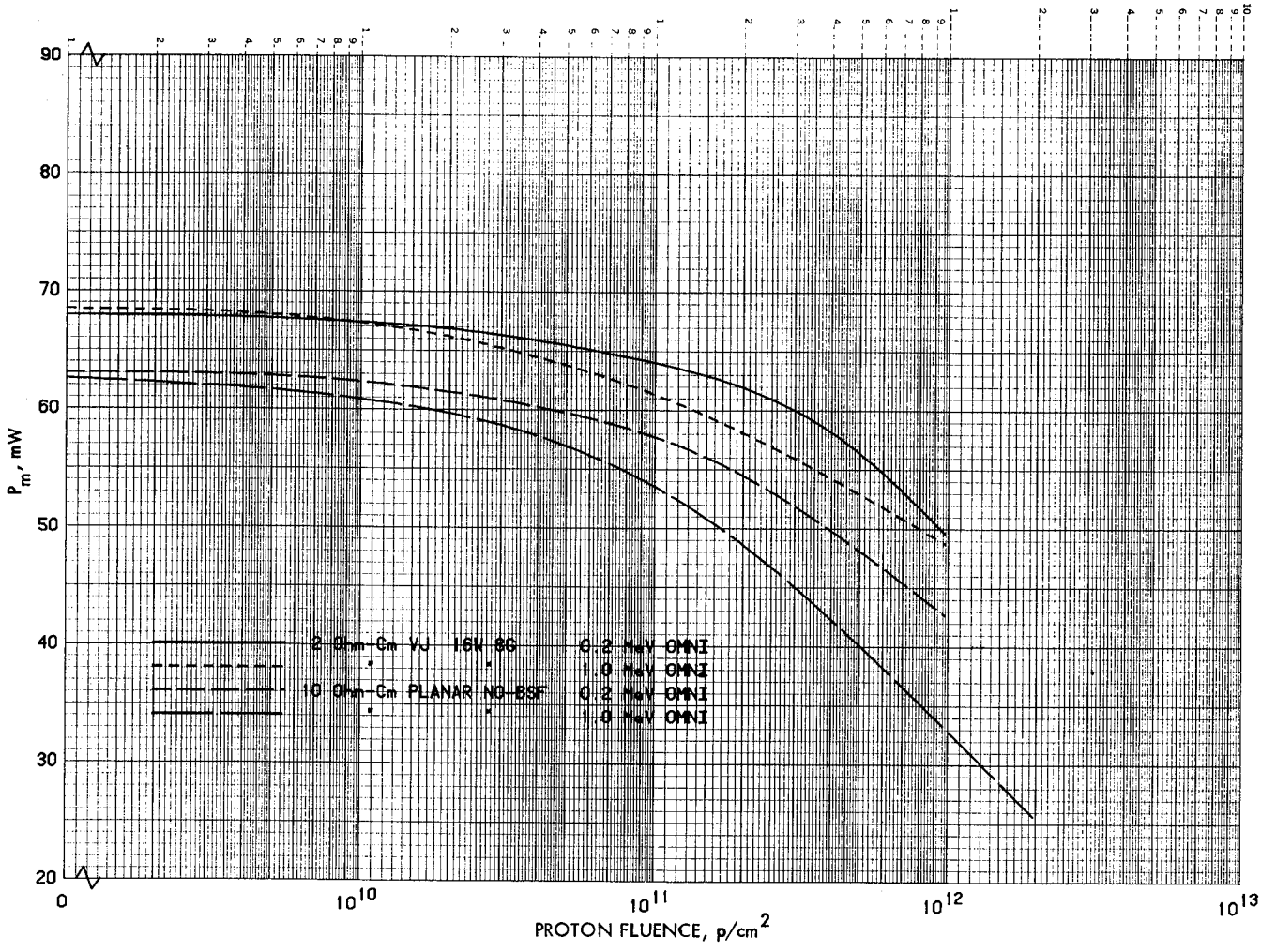

Figure 19. P_m Degradation of Vertical Junction Solar Cells by 0.2 and 1.0 MeV Protons

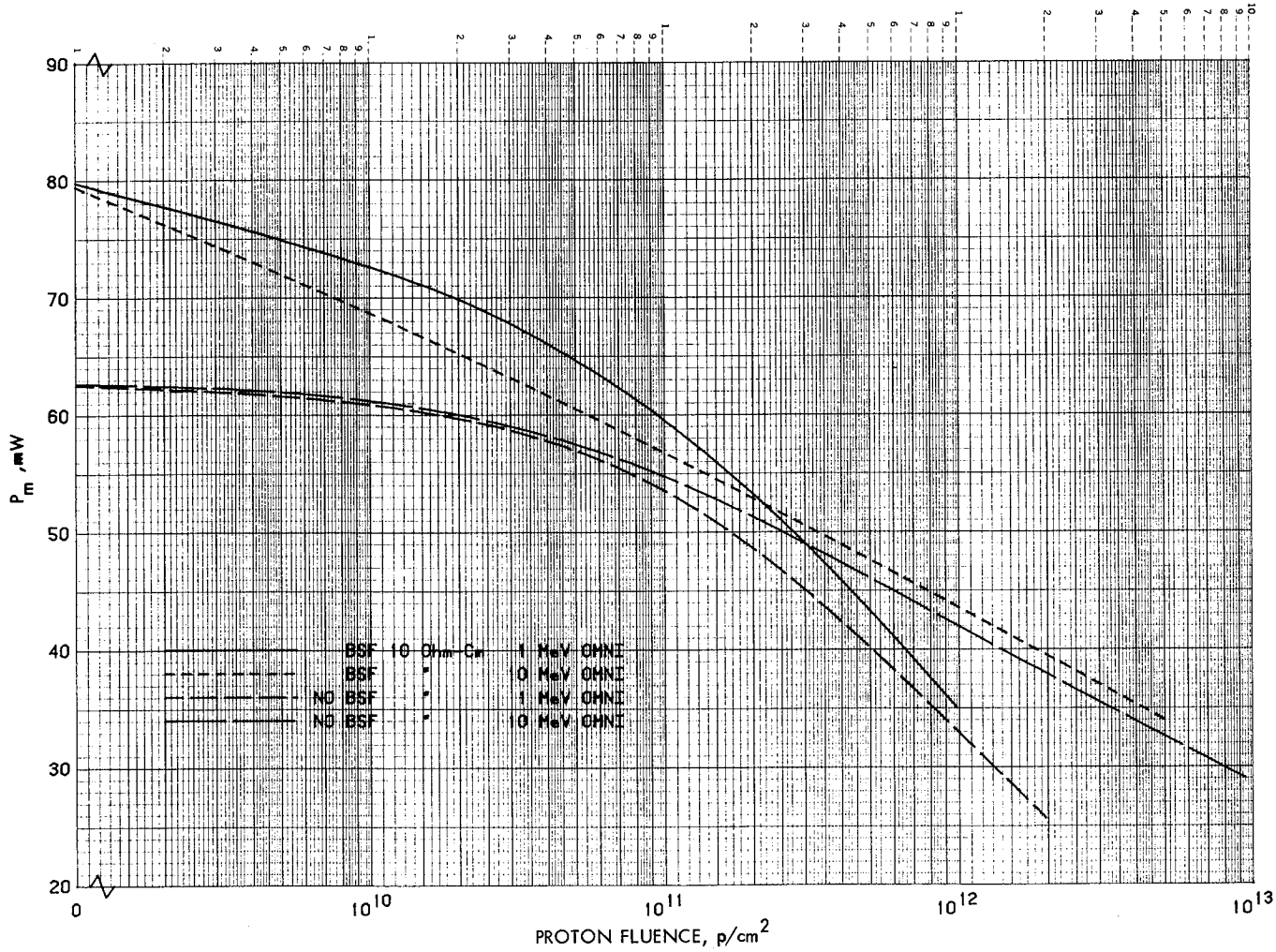

Figure 20. P_m Degradation of BSF Solar Cells by 1.0 and 10 MeV Protons

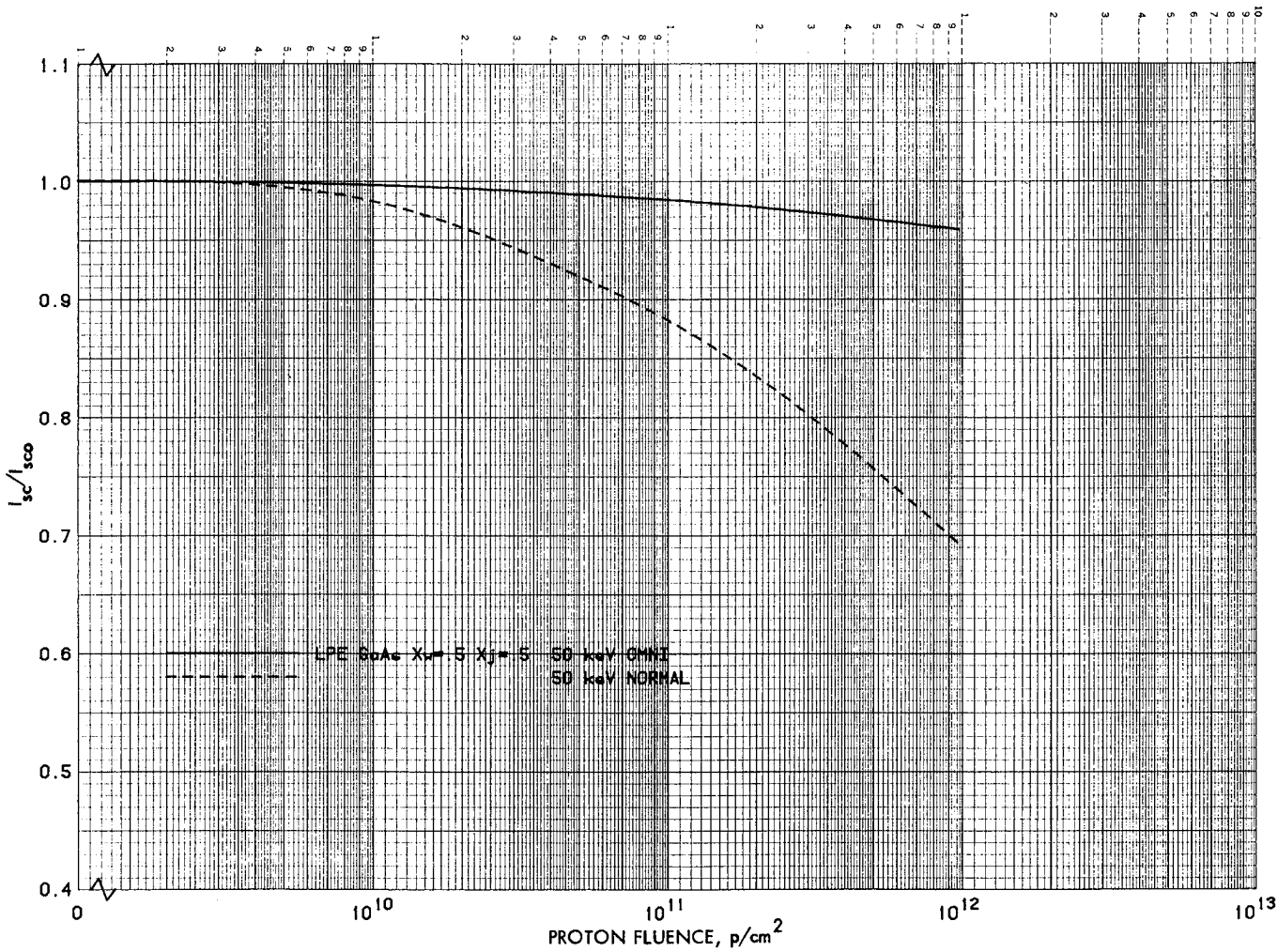

Figure 21. I_{sc} Degradation of GaAs Solar Cells for 50 keV Protons

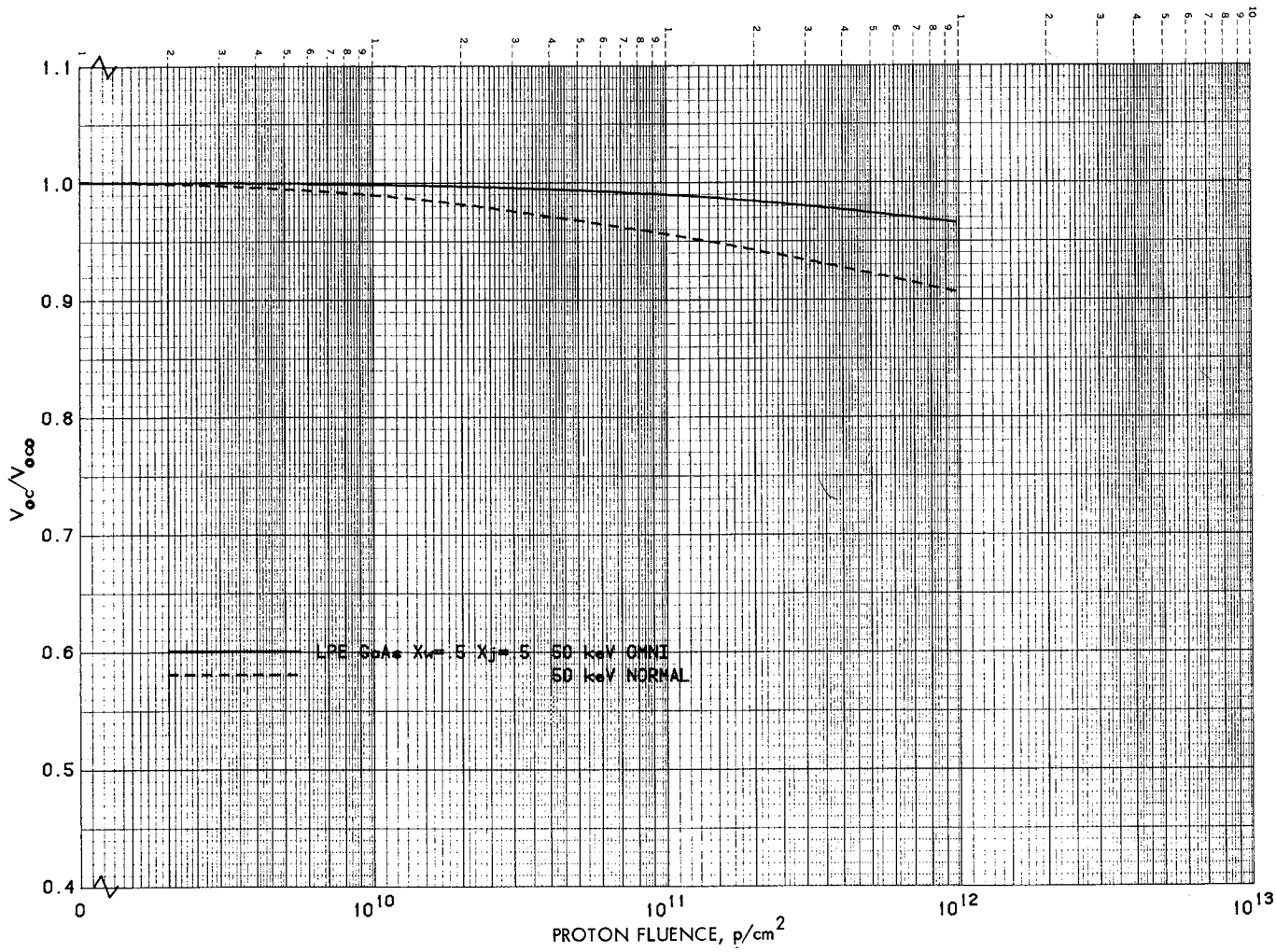

Figure 22. V_{oc} Degradation of GaAs Solar Cells for 50 keV Protons

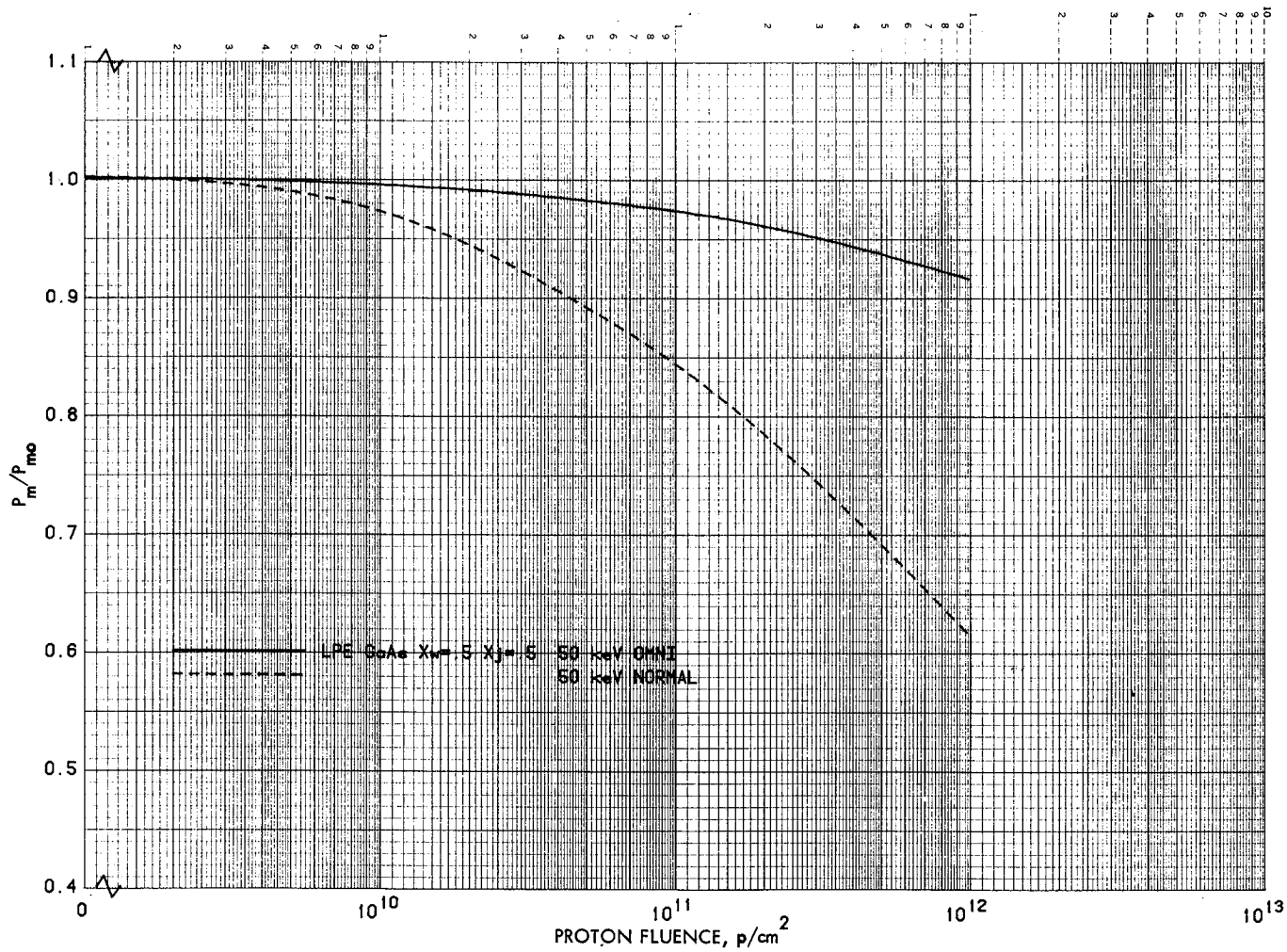

Figure 23. P_m Degradation of GaAs Solar Cells for 50 keV Protons

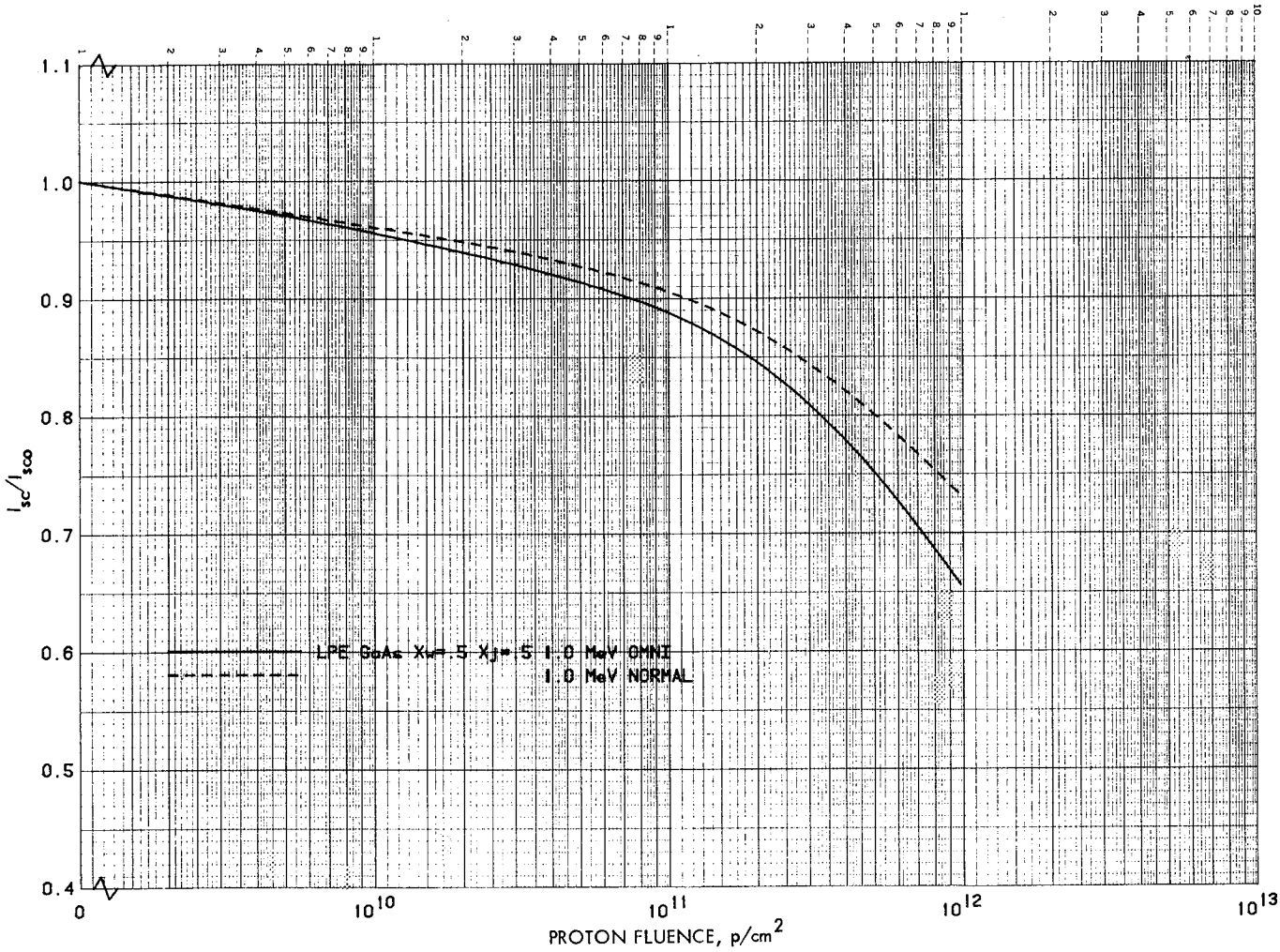

Figure 24. I_{sc} Degradation of GaAs Solar Cells for 1 MeV Protons

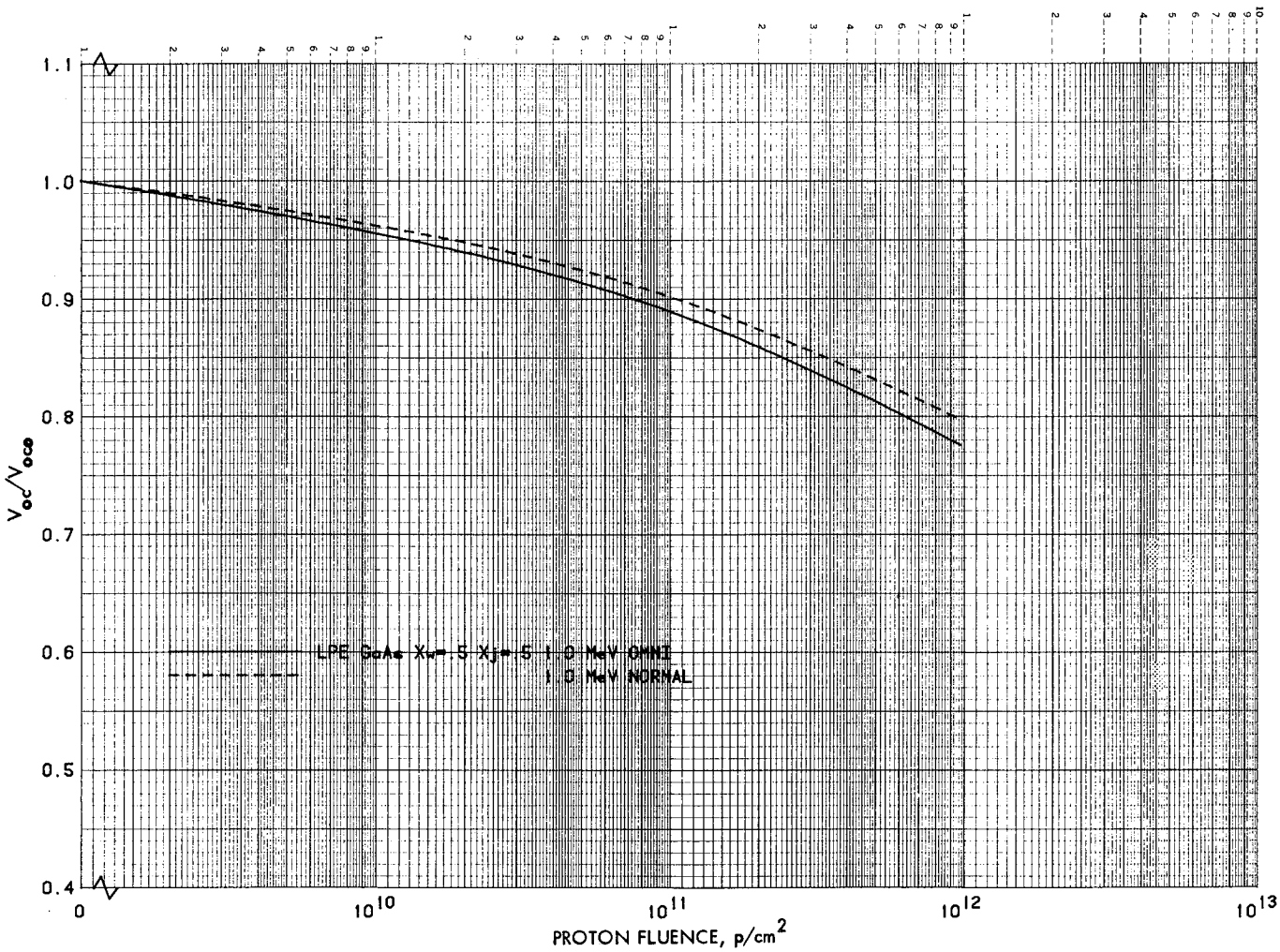

Figure 25. V_{oc} Degradation of GaAs Solar Cells for 1 MeV Protons

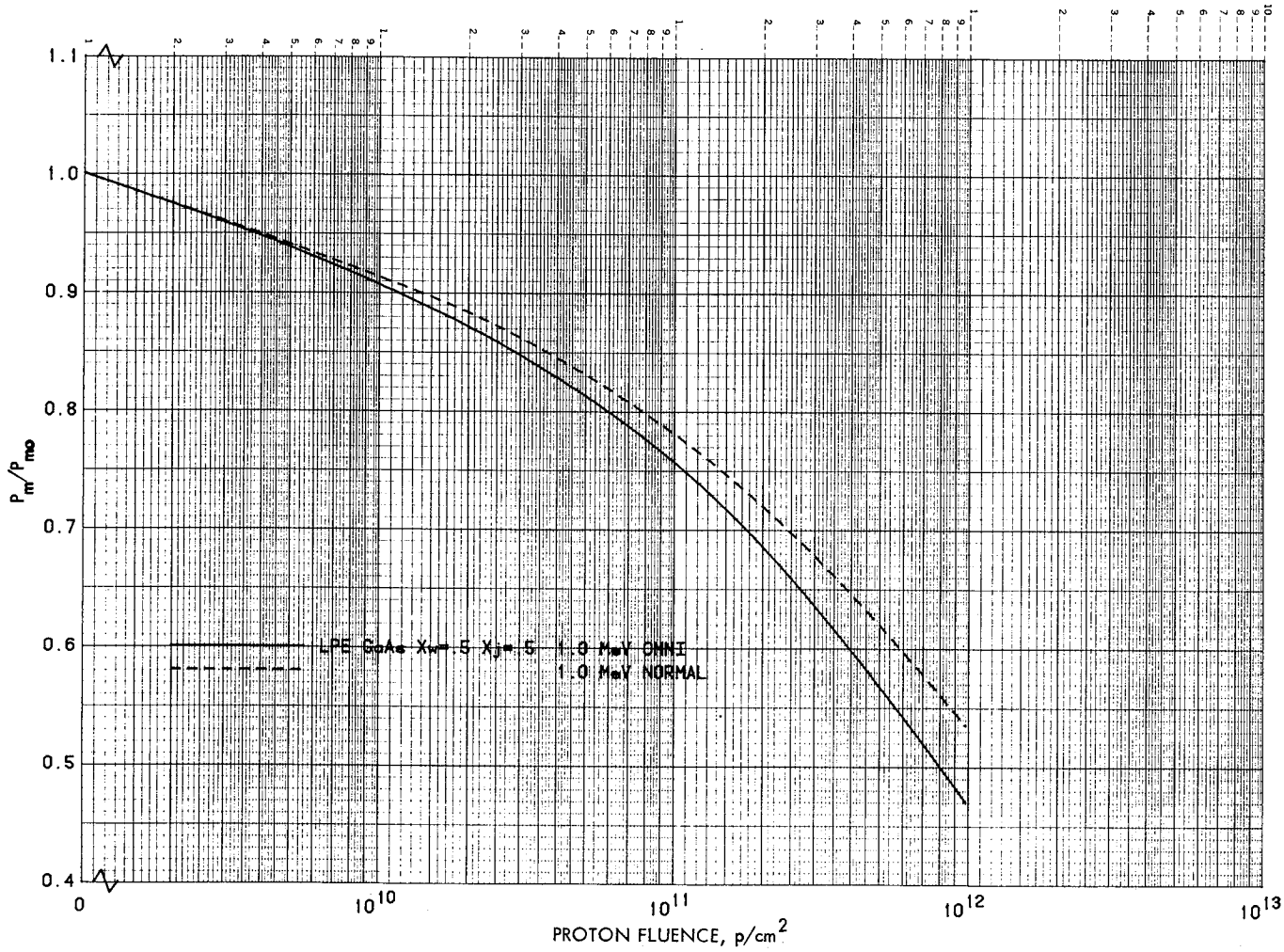

Figure 26. P_m Degradation of GaAs Solar Cells for 1 MeV Protons

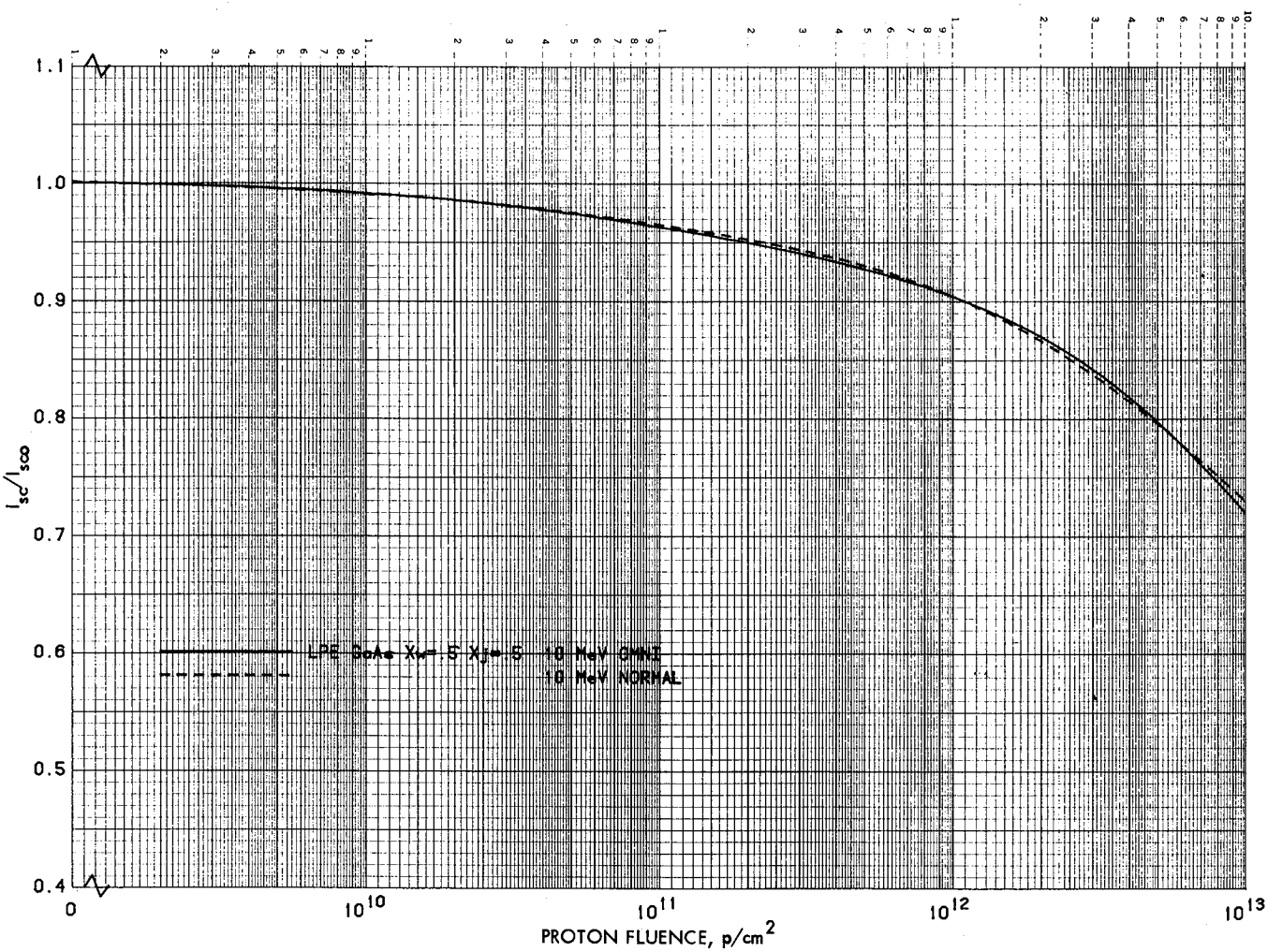

Figure 27. I_{sc} Degradation of GaAs Solar Cells for 10 MeV Protons

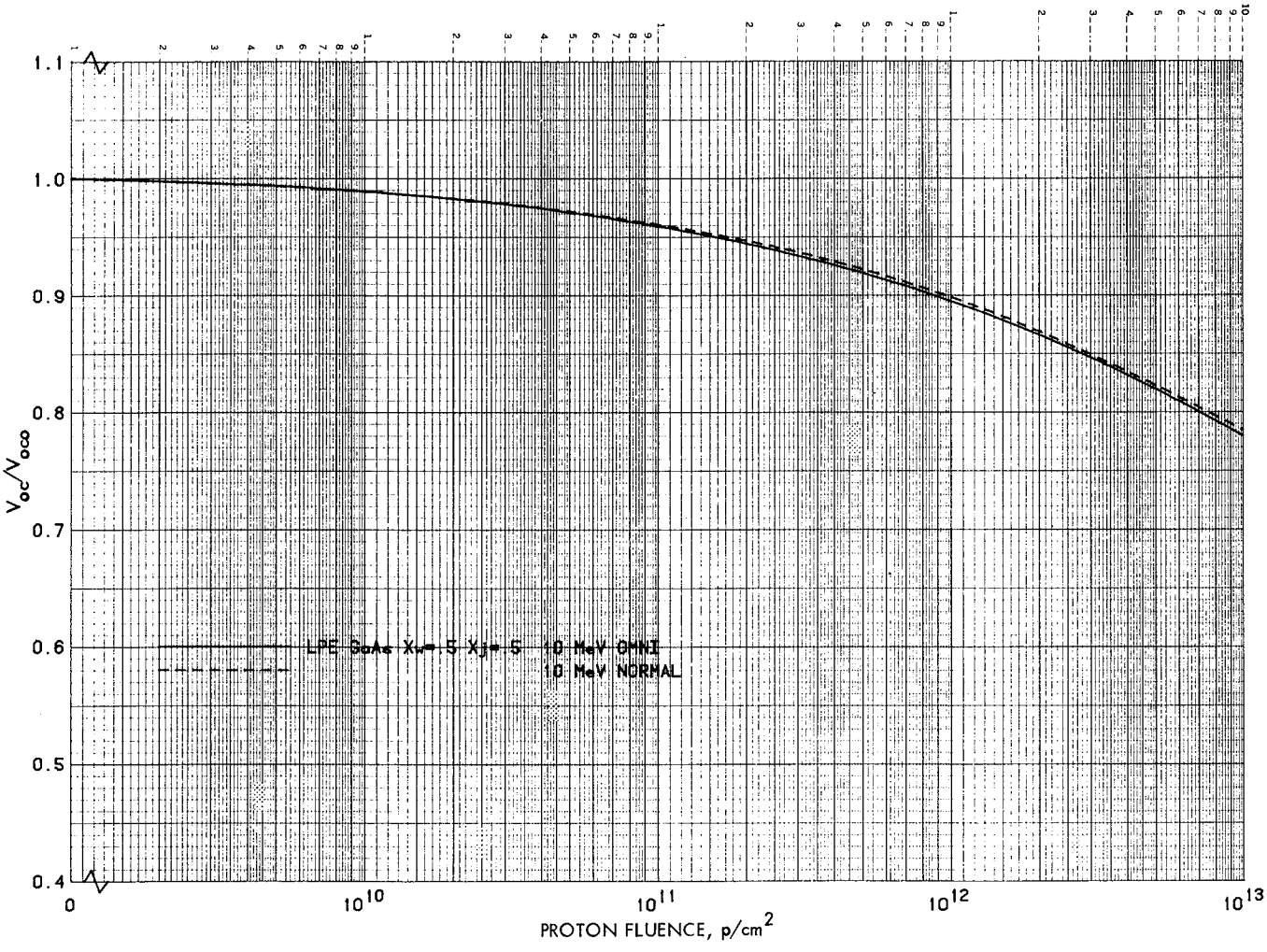

Figure 28. V_{oc} Degradation of GaAs Solar Cells for 10 MeV Protons

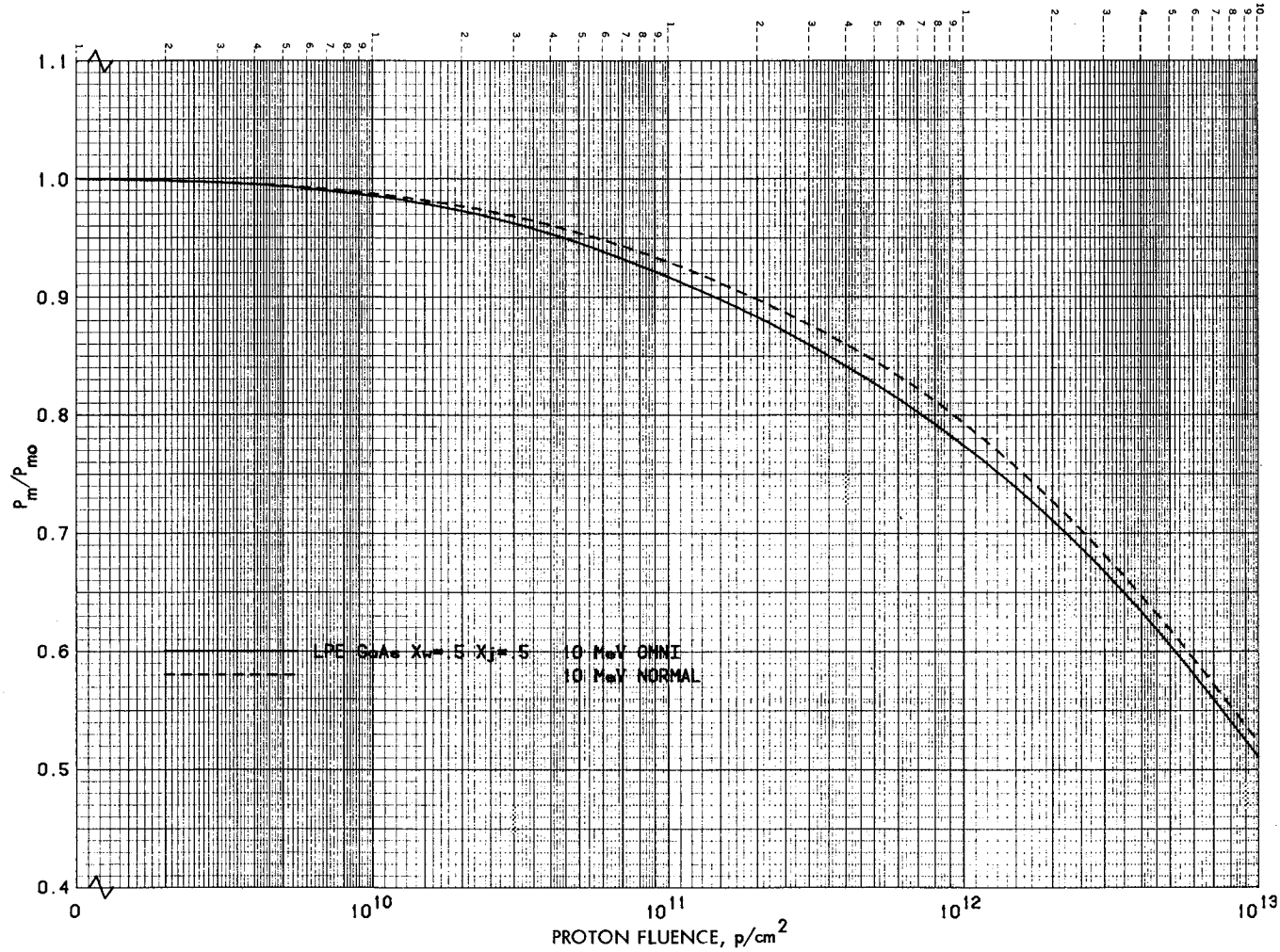

Figure 29. P_m Degradation of GaAs Solar Cells for 10 MeV Protons

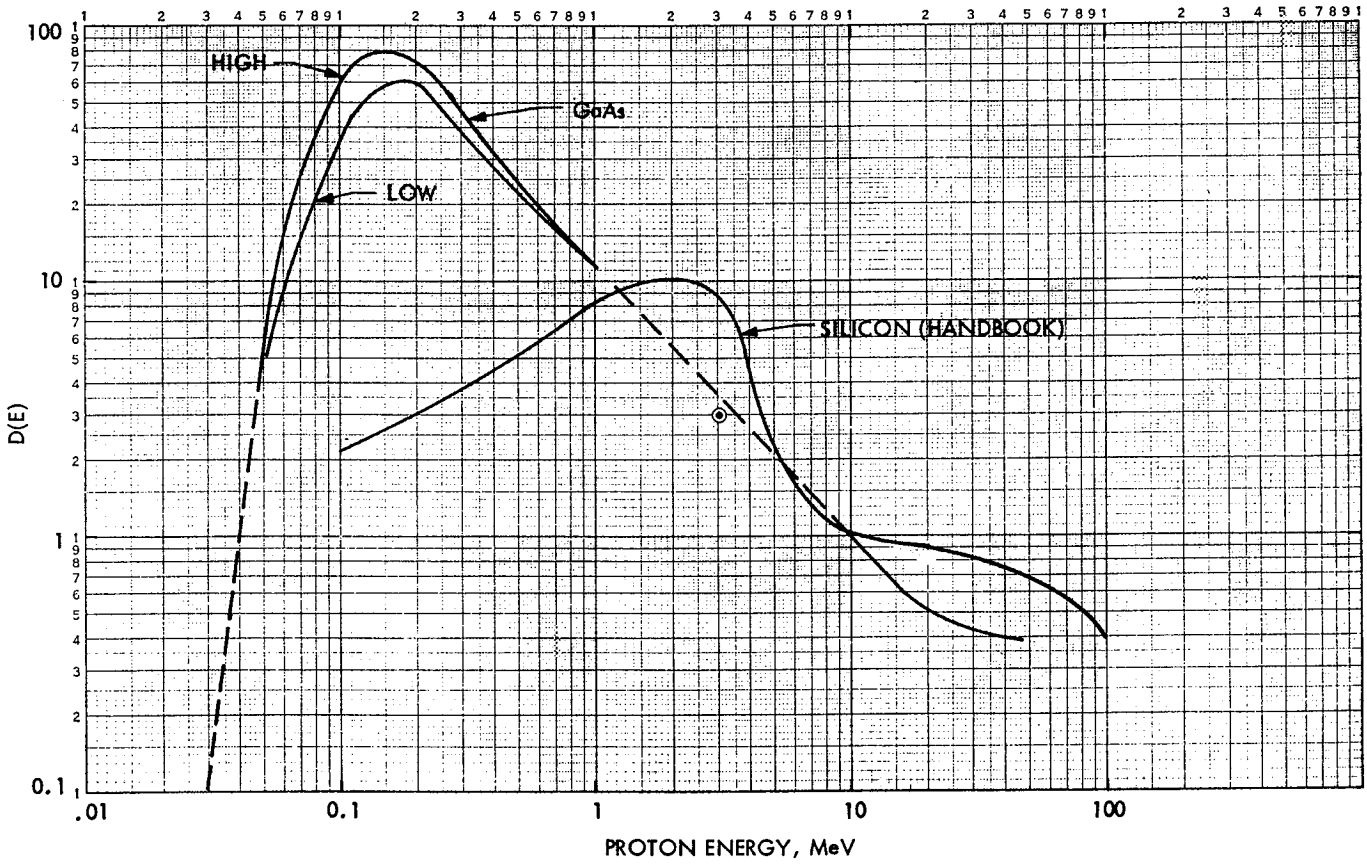

Figure 30. Normal Incidence P_m Damage Coefficients for Si and GaAs

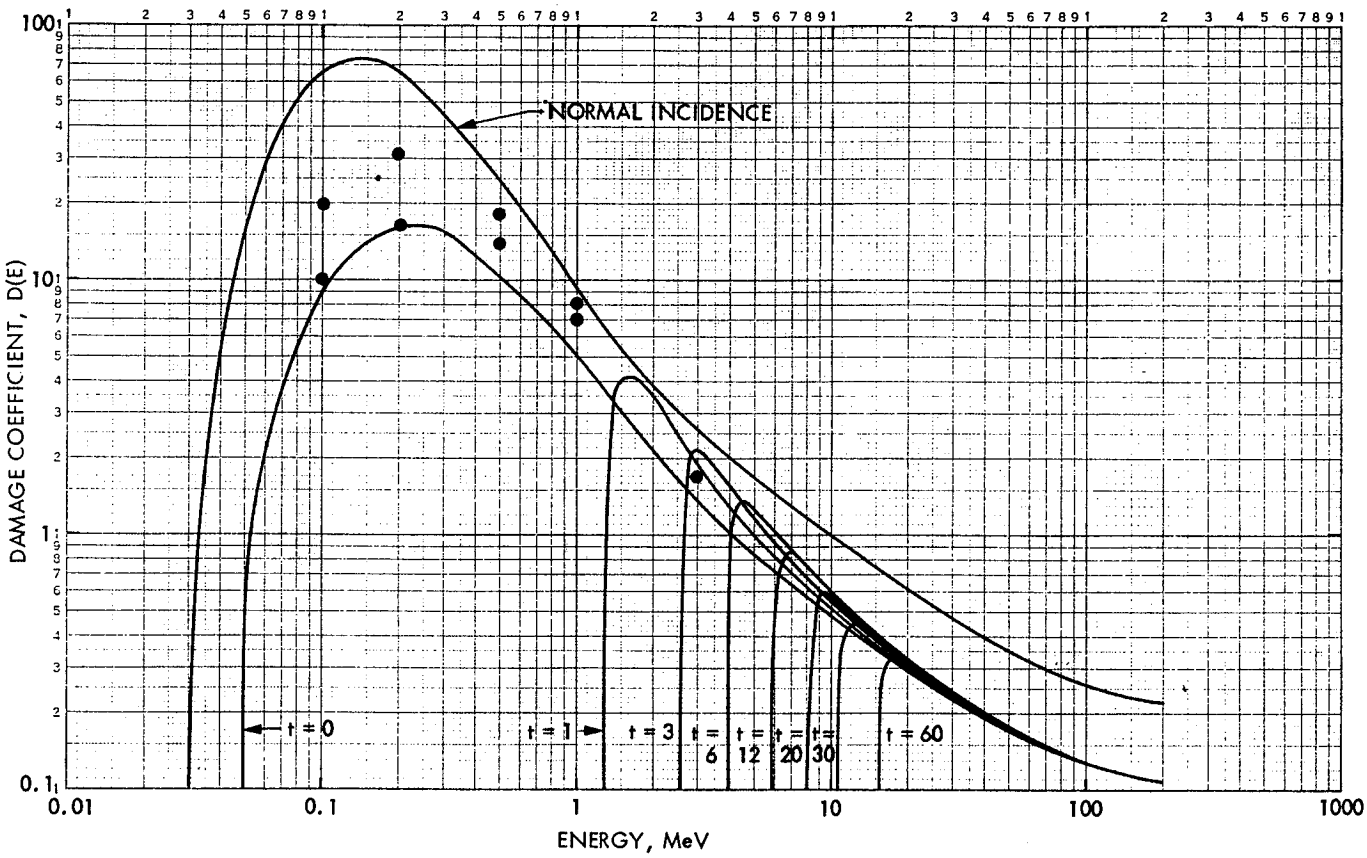

Figure 31. Normal and Omni I_{sc} Damage Coefficients for GaAs

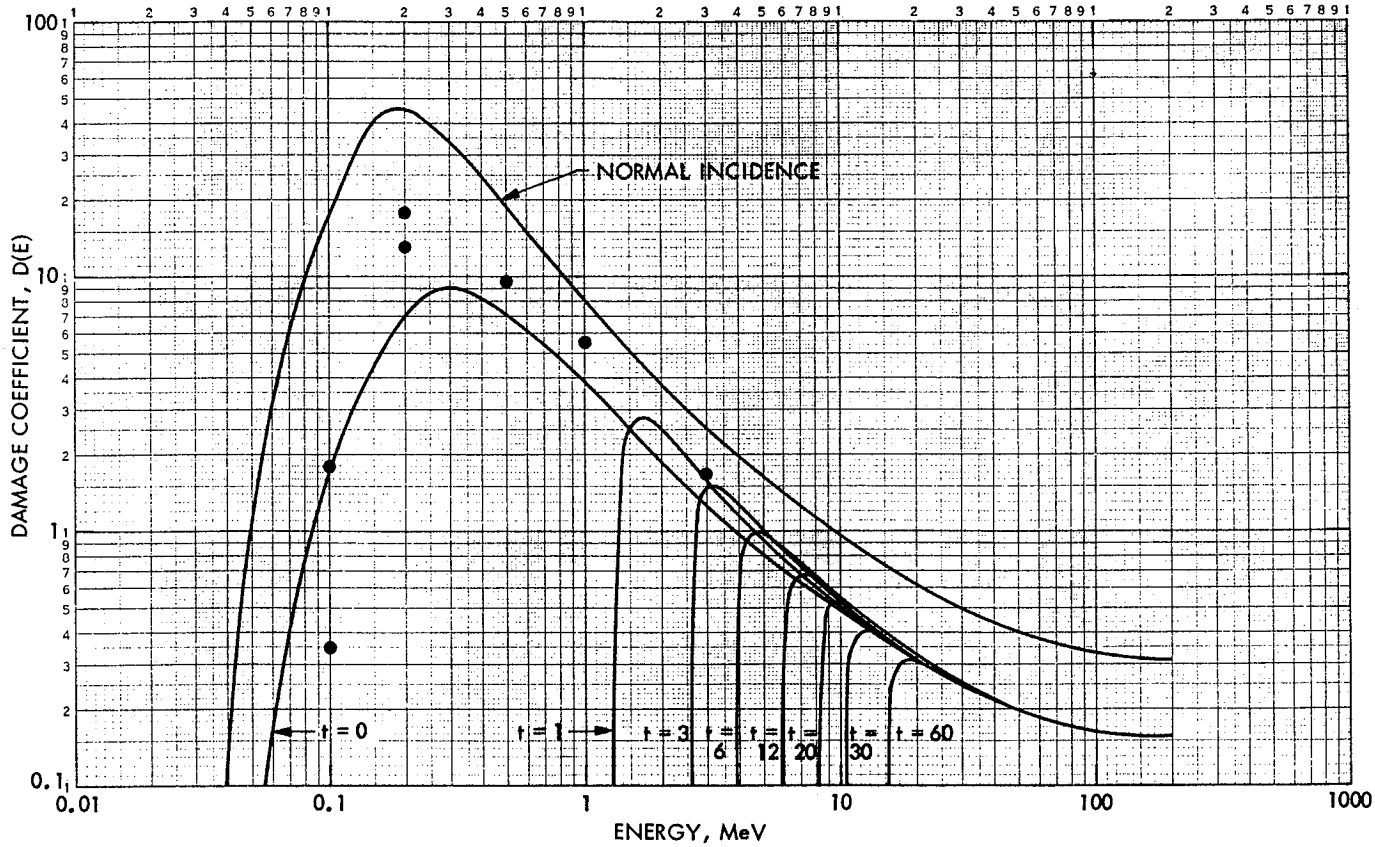

Figure 32. Normal and Omni V_{oc} Damage Coefficients for GaAs

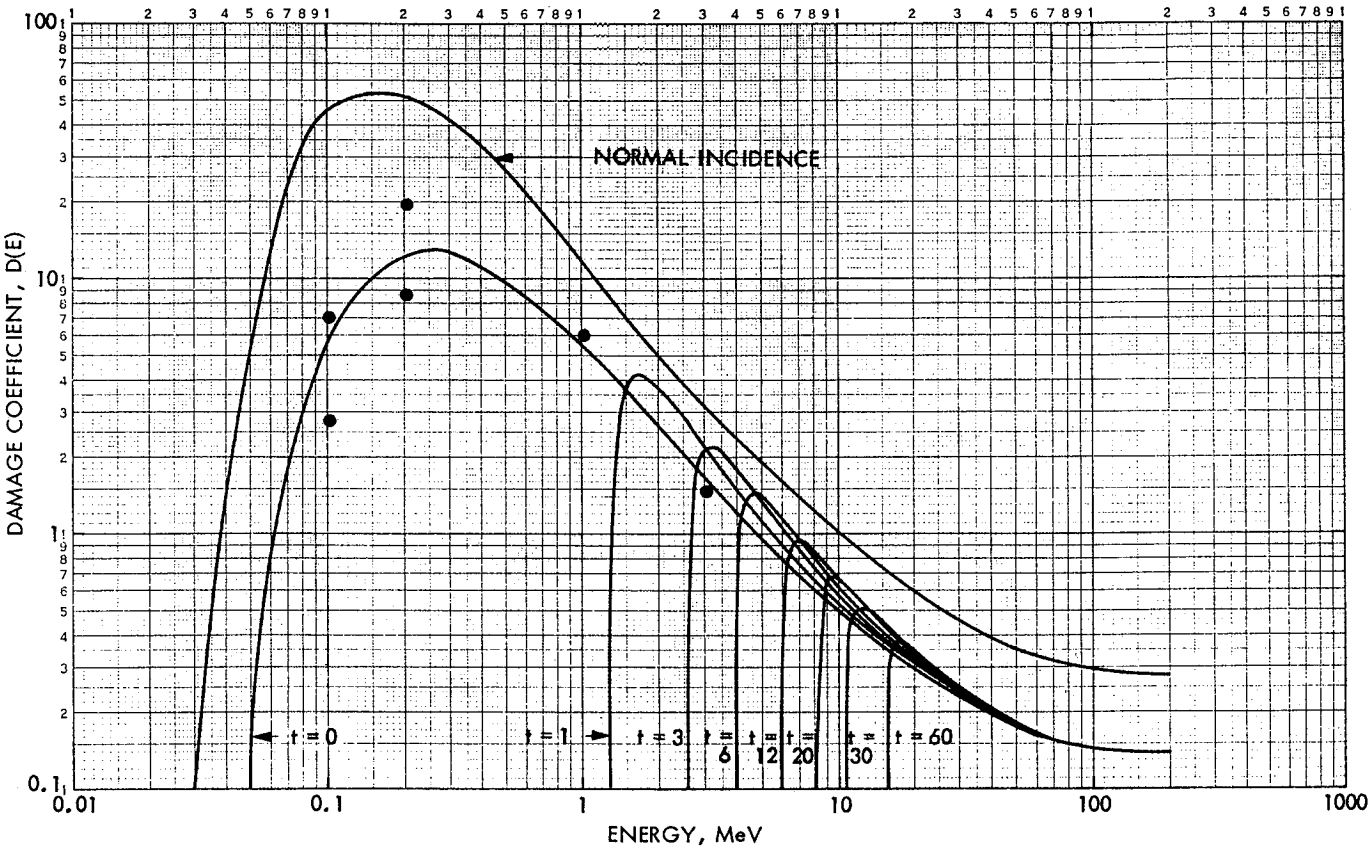

Figure 33. Normal and Omni P_m Damage Coefficients for GaAs

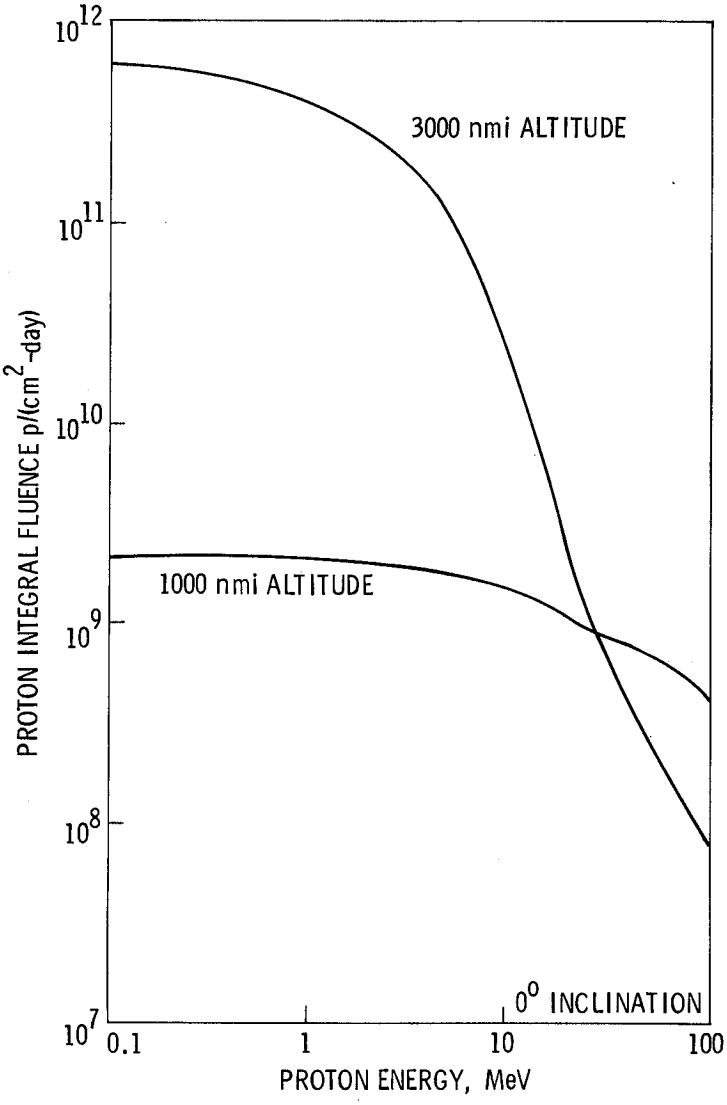

Figure 34. Proton Integral Fluence Spectra for 1000 nmi and 3000 nmi Circular Orbits

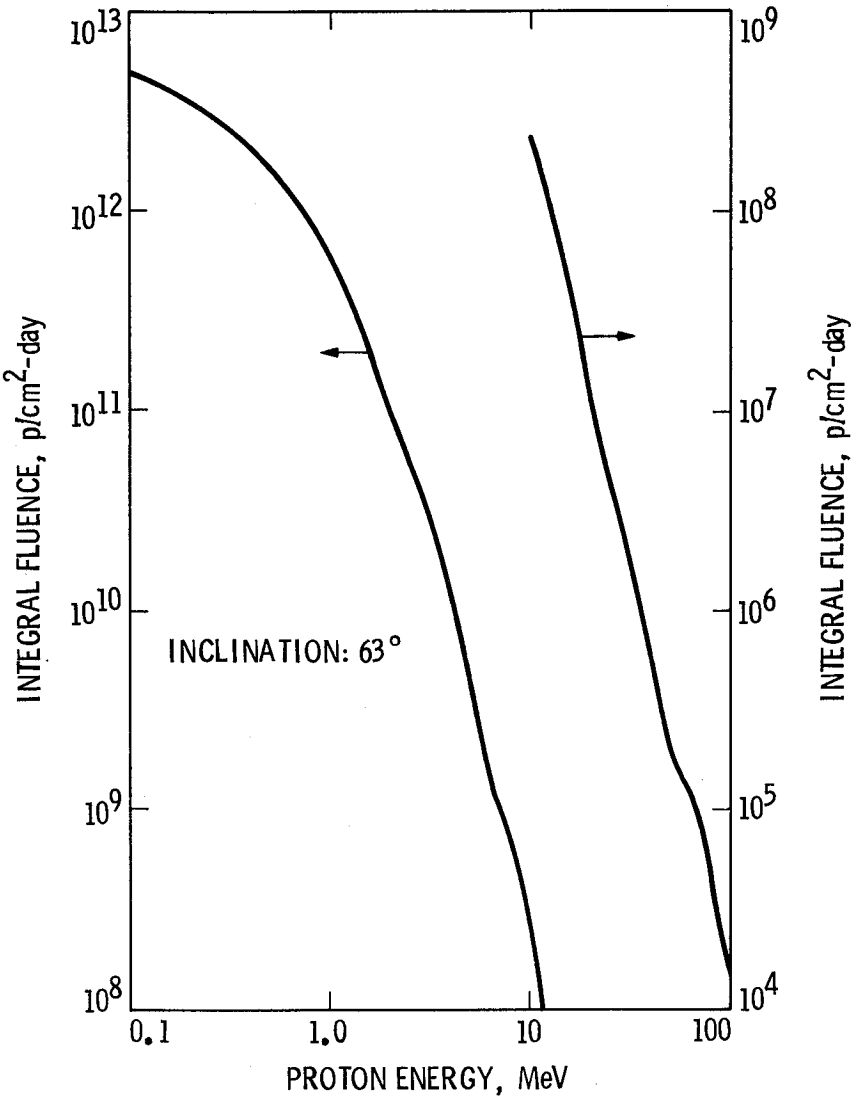

Figure 35. Proton Integral Fluence Spectra for a 5600 nmi Circular Orbit

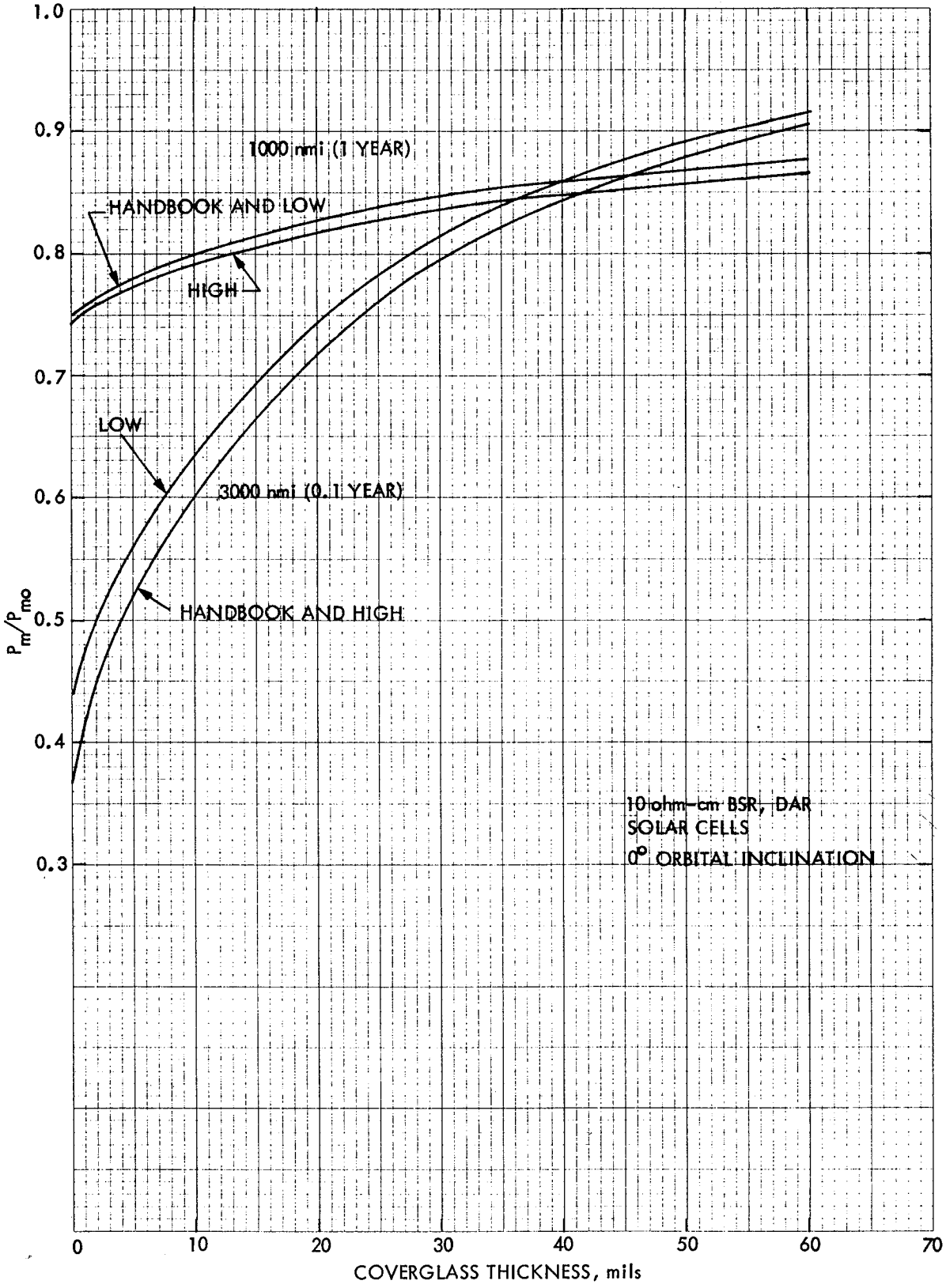

Figure 36. Computed Si Solar Cell P_m Degradation in 1000 nmi and 3000 nmi Orbital Proton Environments

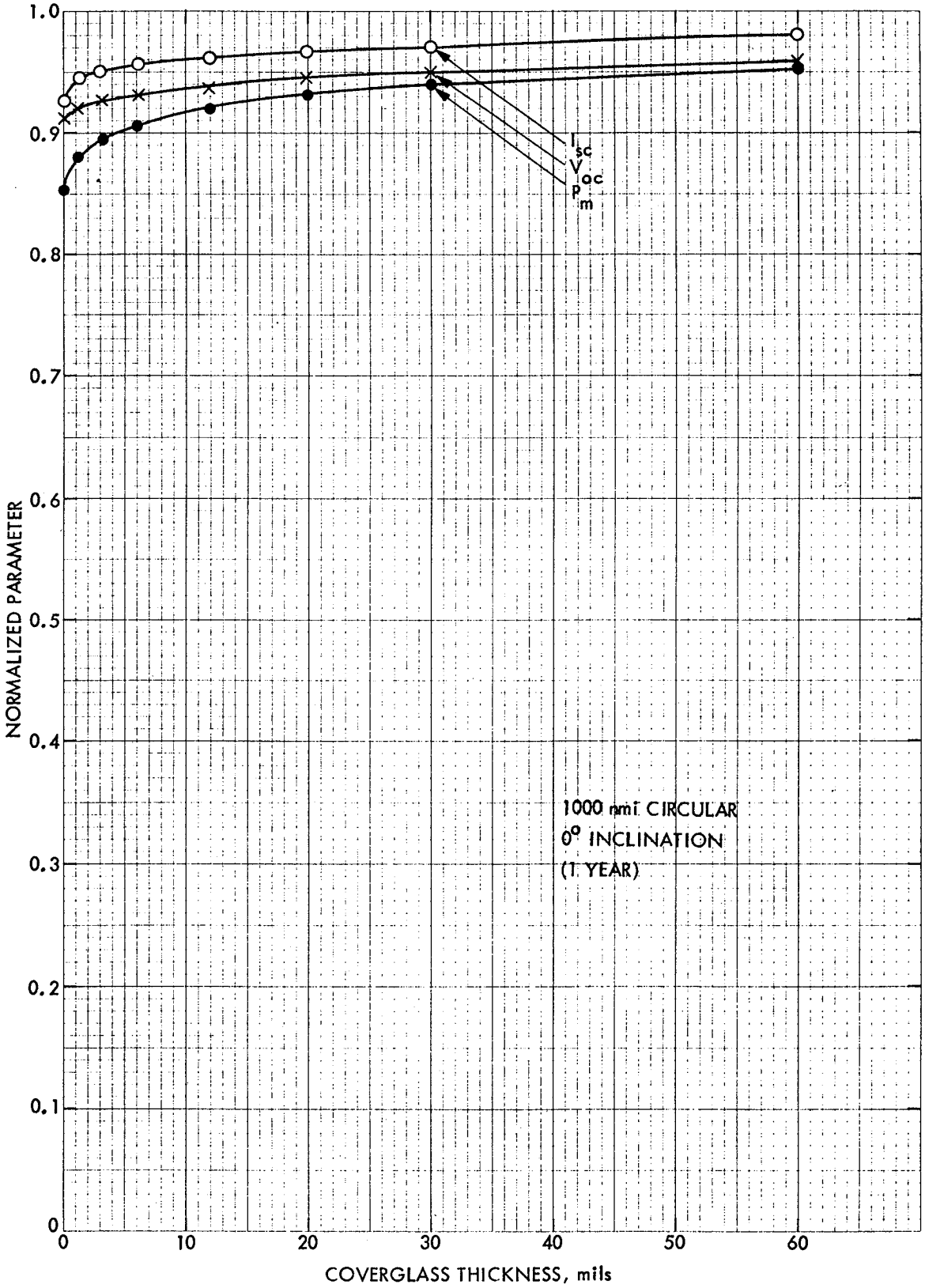

Figure 37. Computed Electrical Parameter Degradation of GaAs Solar Cells in a 1000 nmi Circular Orbit

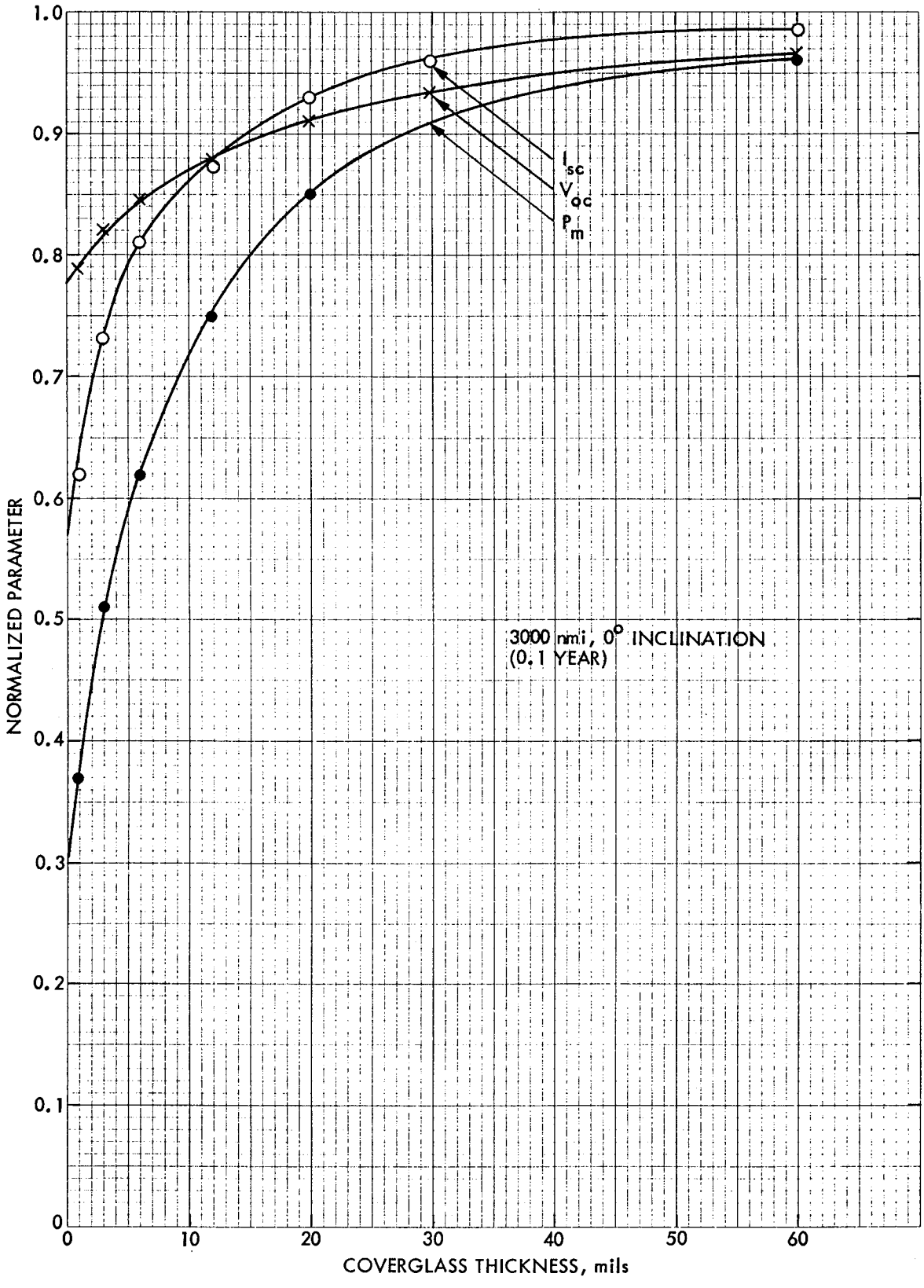

Figure 38. Computed Electrical Parameter Degradation of GaAs Solar Cells in a 3000 nmi Circular Orbit

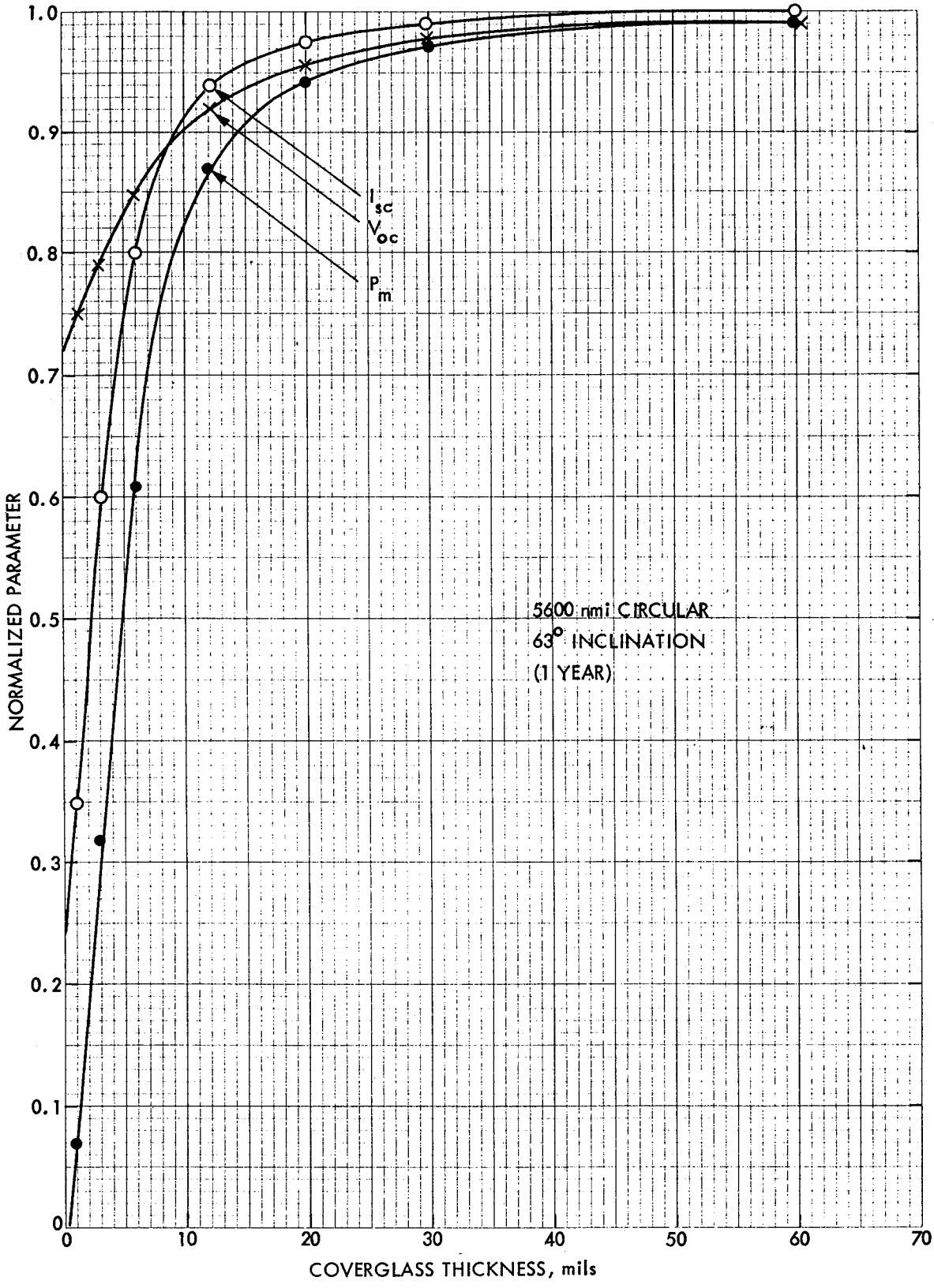

Figure 39. Computed Electrical Parameter Degradation of GaAs Solar Cells in a 5600 nmi Circular Orbit

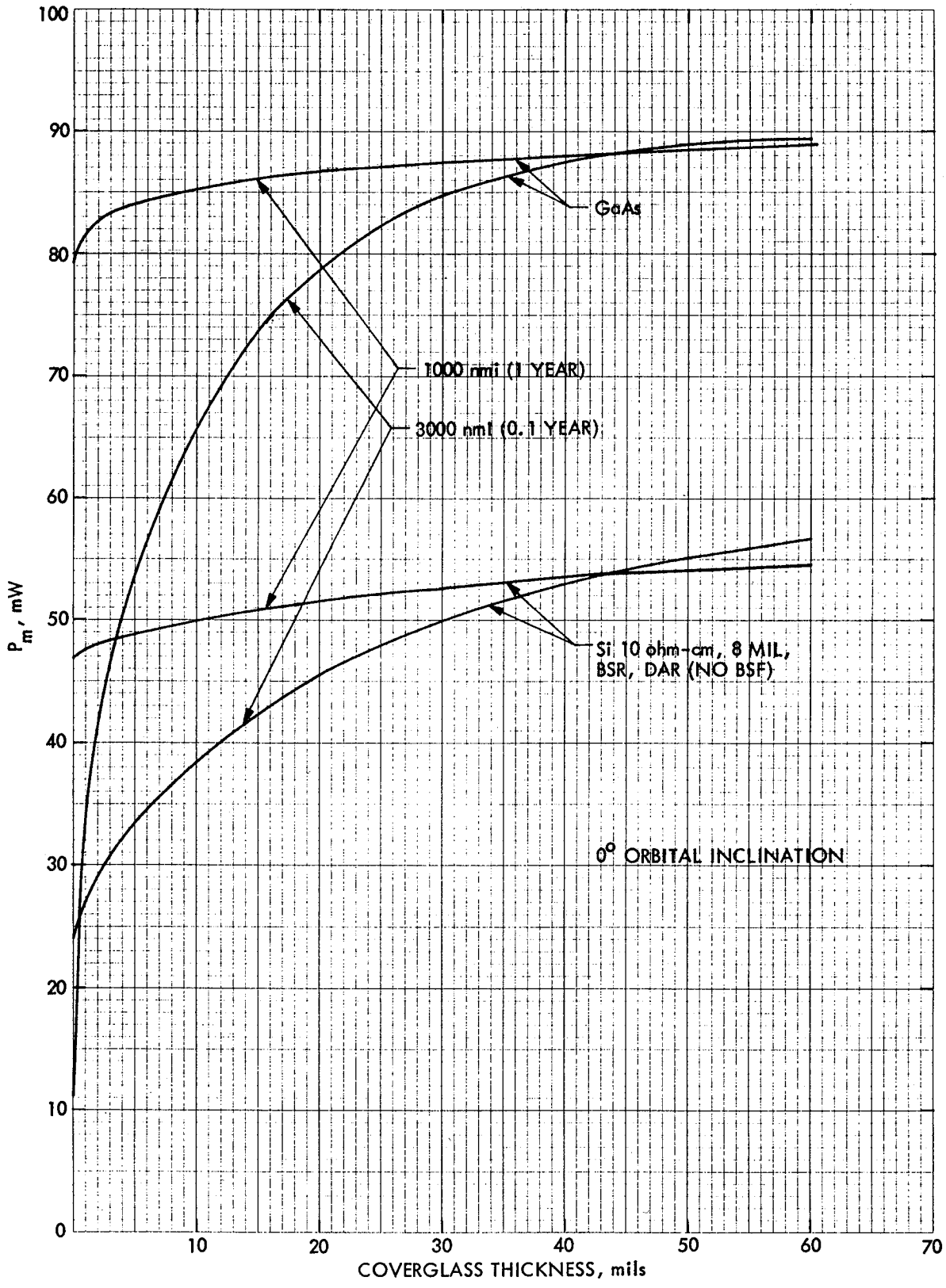

Figure 40. Computed Si and GaAs Solar Cell P_m Degradation in 1000 nmi and 3000 nmi Orbital Proton Environments

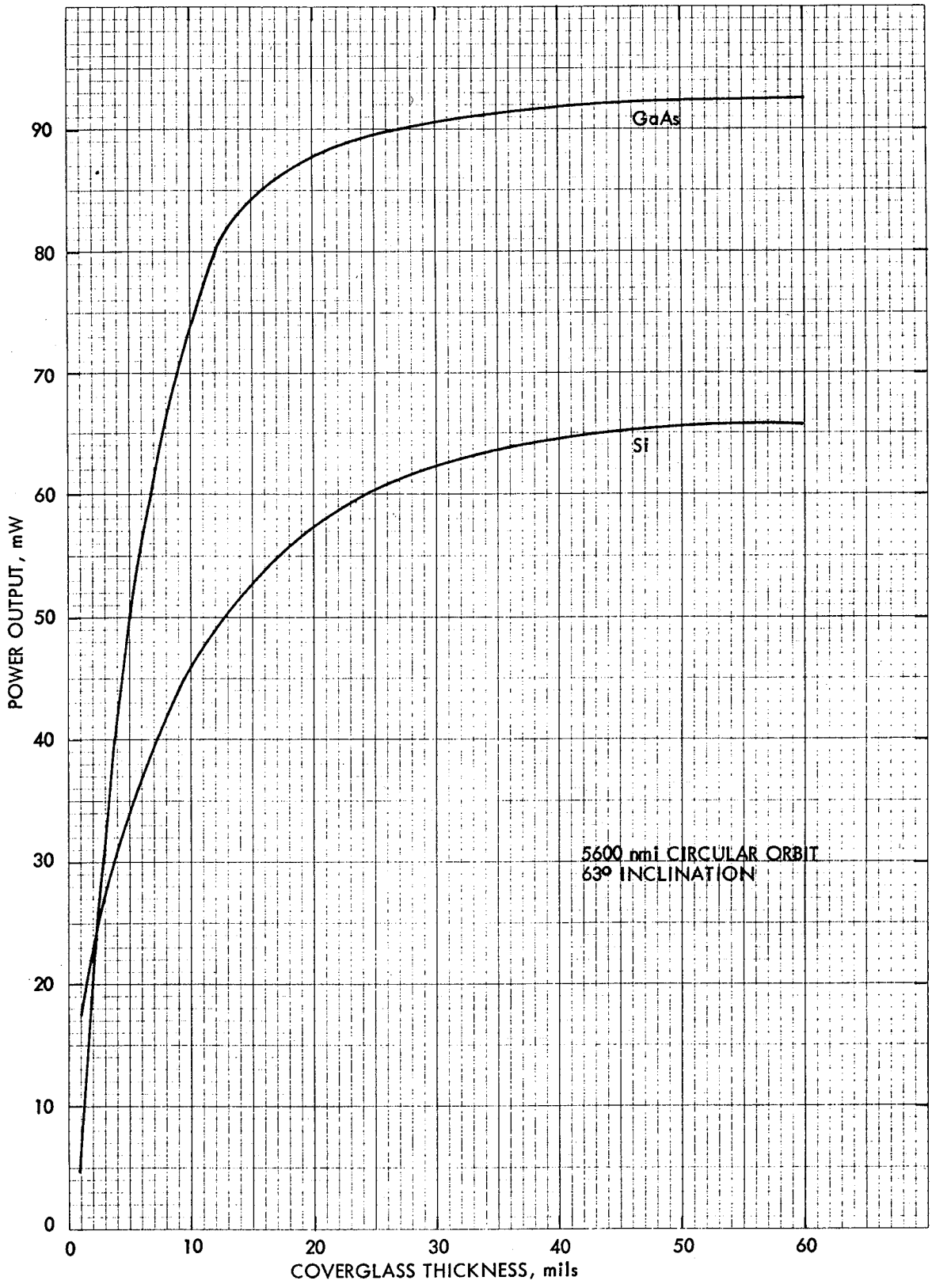

Figure 41. Computed Si and GaAs Solar Cell P_m Degradation in a 5600 nmi Orbital Proton Environment

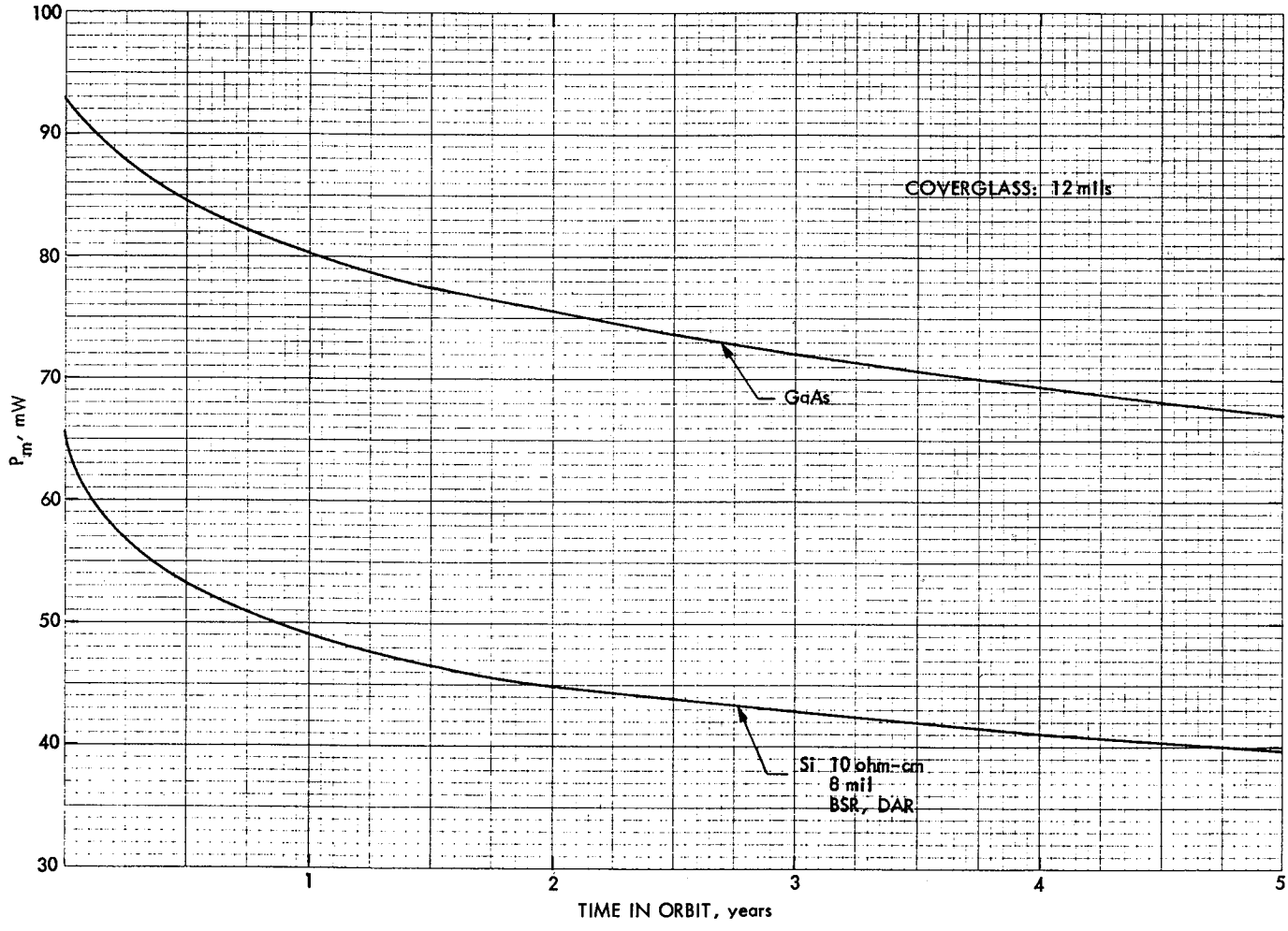

Figure 42. Computed Si and GaAs Solar Cell P_m Degradation vs Time in a 5600 nmi Orbit

APPENDIX

TABLE A1: PROTON TEST 0.05 MEV OMNI IRRADIATION
HRL GaAlAs Xw= 0.5 uM Xj= 0.5 uM 15 MIL BOX 119
Ta2O5 AR COATING
2/84

CELL AREA = 4.000 CM^2

RAD. LEVEL	Isc	Voc	Imp	Vmp	Pmax	FF
*0	110.90	1026.30	104.47	867.80	90.66	0.797
*1E+10	110.80	1024.50	104.10	867.00	90.25	0.795
*2E+10	110.30	1022.90	103.90	865.40	89.92	0.797
*5E+10	109.37	1019.50	102.80	864.10	88.83	0.797
*1E+11	109.50	1016.80	102.57	863.30	88.55	0.795
*2E+11	108.87	1011.10	101.73	858.60	87.35	0.793
*5E+11	107.43	1001.00	101.83	837.60	85.29	0.793
*1E+12	106.07	989.60	99.87	829.30	82.82	0.789
1E+12/ANN(RT95)	106.03	990.60	99.37	835.60	83.03	0.791

PROTON TEST 0.05 MEV NORMAL IRRADIATION
HRL GaAlAs Xw= 0.5 uM Xj= 0.5 uM 15 MIL BOX 119
Ta2O5 AR COATING
2/84

CELL AREA = 4.000 CM^2

RAD. LEVEL	Isc	Voc	Imp	Vmp	Pmax	FF
*0	112.50	1023.00	105.70	868.40	91.79	0.798
*1E+10	110.80	1013.30	104.50	856.20	89.47	0.797
*2E+10	108.43	1005.20	102.17	851.00	86.95	0.798
*5E+10	102.90	988.40	97.17	836.50	81.28	0.799
*1E+11	99.83	978.70	94.37	827.70	78.11	0.799
*2E+11	94.30	965.30	88.10	820.60	72.29	0.794
*5E+11	85.40	945.10	81.37	783.40	63.75	0.790
*1E+12	77.73	926.20	73.47	768.40	56.45	0.784
1E+12/ANN(RT95)	77.70	927.00	73.67	765.70	56.41	0.783

TABLE A2: PROTON TEST .1 MEV OMNI IRRADIATION
HRL GaAlAs Xw=.5 Xj=.5 15 MIL BOX 119
Ta2O5 AR COATING
11/83

CELL AREA = 4.000 CM^2

RAD. LEVEL	Isc	Voc	Imp	Vmp	Pmax	FF
*0	114.73	1026.30	109.20	860.20	93.93	0.798
*1E+10	111.90	1003.20	106.40	836.60	89.01	0.793
*2E+10	109.63	991.40	104.10	825.90	85.98	0.791
*5E+10	104.37	972.70	98.50	811.30	79.91	0.787
*1E+11	96.27	956.30	90.60	802.70	72.72	0.790
*2E+11	84.17	936.20	79.50	779.00	61.93	0.786
*5E+11	70.80	924.50	66.30	772.90	51.24	0.783
*1E+12	56.80	905.40	53.00	753.00	39.91	0.776
1E+12/ANN(RT28)	56.47	905.50	53.10	748.40	39.74	0.777

PROTON TEST .1 MEV NORMAL IRRADIATION
HRL GaAlAs Xw=.5 Xj=.5 15 MIL BOX 119
Ta2O5 AR COATING
11/83

CELL AREA = 4.000 CM^2

RAD. LEVEL	Isc	Voc	Imp	Vmp	Pmax	FF
*0	114.30	1022.80	107.70	868.80	93.57	0.800
*1E+10	107.70	961.70	102.00	799.70	81.57	0.788
*2E+10	102.00	943.40	96.00	787.10	75.56	0.785
*5E+10	89.70	915.00	84.60	754.60	63.84	0.778
*1E+11	74.57	889.50	69.90	731.00	51.10	0.770
*2E+11	59.45	876.20	55.60	715.10	39.76	0.763
*5E+11	47.20	848.00	43.90	702.70	30.85	0.771
*1E+12	39.40	844.60	35.90	697.10	25.03	0.752
1E+12/ANN(RT28)	39.30	846.40	36.95	671.50	24.81	0.746

TABLE A3: PROTON TEST 0.2 MEV OMNI IRRADIATION
HRL GaAlAs Xw= 0.5 uM Xj= 0.5 uM 15 MIL BOX 119
Ta2O5 AR COATING
2/84

CELL AREA = 4.000 CM^2

RAD. LEVEL	Isc	Voc	Imp	Vmp	Pmax	FF
*0	113.93	1022.60	107.00	861.30	92.16	0.791
*1E+10	110.03	951.20	103.70	787.50	81.66	0.780
*2E+10	107.23	932.00	100.60	765.00	76.96	0.770
*5E+10	97.73	886.60	90.70	724.50	65.71	0.758
*1E+11	88.83	859.60	82.13	697.40	57.28	0.750
*2E+11	75.70	822.10	68.90	669.30	46.11	0.741
*5E+11	53.87	764.50	48.93	609.30	29.81	0.724
*1E+12	37.10	710.10	34.53	515.10	17.79	0.675
1E+12/ANN(RT95)	37.17	721.40	33.57	556.70	18.69	0.697

PROTON TEST 0.2 MEV NORMAL IRRADIATION
HRL GaAlAs Xw= 0.5 uM Xj= 0.5 uM 15 MIL BOX 119
Ta2O5 AR COATING
2/84

CELL AREA = 4.000 CM^2

RAD. LEVEL	Isc	Voc	Imp	Vmp	Pmax	FF
*0	114.50	1025.00	107.45	864.90	92.93	0.792
*1E+10	106.80	932.10	99.77	772.40	77.06	0.774
*2E+10	102.80	911.50	96.25	752.00	72.38	0.772
*5E+10	94.20	862.50	87.75	702.00	61.60	0.758
*1E+11	87.35	832.40	80.75	674.50	54.47	0.749
*2E+11	76.65	793.30	70.05	642.60	45.01	0.740
*5E+11	56.90	731.20	51.95	578.30	30.04	0.722
*1E+12	40.55	679.40	37.90	495.00	18.76	0.681
1E+12/ANN(RT95)	40.20	691.00	36.40	537.90	19.58	0.705

TABLE A4: PROTON TEST .5 MEV OMNI IRRADIATION
HRL GaAlAs Xw= 0.5 uM Xj= 0.5 uM 15 MIL BOX 119
Ta2O5 AR COATING
11/83

CELL AREA = 4.000 CM^2

RAD. LEVEL	Isc	Voc	Imp	Vmp	Pmax	FF
*0	113.87	1022.60	106.90	866.30	92.61	0.795
*1E+10	106.27	964.20	99.70	812.90	81.05	0.791
*2E+10	103.80	947.70	97.30	794.20	77.28	0.786
*5E+10	100.43	919.20	93.90	762.30	71.58	0.775
*1E+11	95.73	890.20	88.90	731.90	65.07	0.764
*2E+11	89.67	856.70	83.20	697.10	58.00	0.755
*5E+11	76.93	801.60	70.80	642.90	45.52	0.738
*1E+12	64.10	756.60	57.80	609.80	35.25	0.727
1E+12/ANN(RT32)	64.23	764.10	57.83	618.50	35.77	0.729

PROTON TEST .5 MEV NORMAL IRRADIATION
HRL GaAlAs Xw= 0.5 uM Xj= 0.5 uM 15 MIL BOX 119
Ta2O5 AR COATING
11/83

CELL AREA = 4.000 CM^2

RAD. LEVEL	Isc	Voc	Imp	Vmp	Pmax	FF
*0	112.33	1019.80	106.40	873.00	92.89	0.811
*1E+10	106.80	967.20	100.60	815.30	82.02	0.794
*2E+10	104.57	951.80	98.20	803.60	78.91	0.793
*5E+10	101.60	925.20	95.50	767.30	73.28	0.780
*1E+11	97.30	897.10	90.80	750.60	68.15	0.781
*2E+11	91.30	862.20	84.90	698.70	59.32	0.754
*5E+11	78.47	807.70	72.30	649.00	46.92	0.740
*1E+12	64.97	763.60	59.30	608.40	36.08	0.727
1E+12/ANN(RT32)	64.70	769.80	58.97	613.50	36.18	0.726

TABLE A5: PROTON TEST 1.0 MEV OMNI IRRADIATION
HRL GaAlAs Xw= 0.5 uM Xj= 0.5 uM 15 MIL BOX 119
Ta2O5 AR COATING
11/83

CELL AREA = 4.000 CM^2

RAD. LEVEL	Isc	Voc	Imp	Vmp	Pmax	FF
*0	113.97	1026.70	107.30	864.97	92.81	0.793
*1E+10	108.90	980.50	102.20	822.90	84.10	0.788
*2E+10	107.00	964.80	100.80	799.70	81.01	0.785
*5E+10	104.10	939.20	97.40	773.80	75.37	0.771
*1E+11	101.23	914.70	94.20	749.00	70.56	0.762
*2E+11	96.57	884.00	90.50	709.00	64.16	0.752
*5E+11	86.17	836.80	80.00	664.30	53.14	0.737
*1E+12	74.53	793.50	68.40	631.50	43.19	0.730
1E+12/ANN(RT28)	74.37	798.90	68.97	624.80	43.09	0.725

PROTON TEST 1.0 MEV NORMAL IRRADIATION
HRL GaAlAs Xw= 0.5 uM Xj= 0.5 uM 15 MIL BOX 119
Ta2O5 AR COATING
11/83

CELL AREA = 4.000 CM^2

RAD. LEVEL	Isc	Voc	Imp	Vmp	Pmax	FF
*0	114.10	1024.80	107.80	861.10	92.83	0.794
*1E+10	109.53	985.40	103.10	820.10	84.55	0.783
*2E+10	108.20	972.30	101.60	810.20	82.32	0.782
*5E+10	105.73	948.80	99.00	780.10	77.23	0.770
*1E+11	103.30	925.20	96.60	750.20	72.47	0.758
*2E+11	99.83	898.10	93.20	721.70	67.26	0.750
*5E+11	91.93	854.20	85.10	682.10	58.05	0.739
*1E+12	83.07	814.40	76.20	647.20	49.32	0.729
1E+12/ANN(RT28)	82.37	818.50	76.70	642.20	49.26	0.731

TABLE A6: PROTON TEST 3.0 MEV OMNI IRRADIATION
HRL GaAlAs Xw= 0.5 uM Xj= 0.5 uM 15 MIL BOX 119
Ta2O5 AR COATING
4/84

CELL AREA = 4.000 CM^2

RAD. LEVEL	Isc	Voc	Imp	Vmp	Pmax	FF
*0	113.83	1025.10	107.57	857.70	92.26	0.791
*2E+10	110.03	990.40	103.60	836.60	86.67	0.795
*5E+10	108.20	971.30	102.33	810.40	82.93	0.789
*1E+11	106.70	954.60	100.63	792.70	79.77	0.783
*2E+11	104.43	934.20	97.00	781.70	75.82	0.777
*5E+11	99.63	898.20	93.17	733.00	68.29	0.763
*1E+12	94.63	865.10	87.73	701.40	61.53	0.752
*2E+12	87.23	827.20	81.27	657.50	53.44	0.741
*5E+12	71.97	766.90	66.67	594.40	39.63	0.718
*1E+13	56.33	718.30	51.60	551.10	28.44	0.703

PROTON TEST 3.0 MEV NORMAL IRRADIATION
HRL GaAlAs Xw= 0.5 uM Xj= 0.5 uM 15 MIL BOX 119
Ta2O5 AR COATING
4/84

CELL AREA = 4.000 CM^2

RAD. LEVEL	Isc	Voc	Imp	Vmp	Pmax	FF
*0	114.13	1023.10	108.47	859.60	93.24	0.799
*2E+10	111.40	997.20	105.83	842.80	89.19	0.803
*5E+10	109.70	978.50	103.77	823.30	85.43	0.796
*1E+11	108.27	964.50	103.07	798.70	82.32	0.788
*2E+11	106.60	946.20	100.26	787.00	78.90	0.782
*5E+11	101.83	910.70	95.63	744.60	71.21	0.768
*1E+12	97.20	876.20	91.43	701.70	64.16	0.753
*2E+12	91.93	842.30	85.47	671.40	57.38	0.741
*5E+12	77.37	780.10	71.63	608.00	43.55	0.722
*1E+13	63.73	736.40	57.83	574.60	33.23	0.708

TABLE A7: PROTON TEST 10.0 MEV OMNI IRRADIATION
HRL GaAlAs Xw= 0.5 uM Xj= 0.5 uM 15 MIL BOX 119
Ta2O5 AR COATING
4/84

CELL AREA = 4.000 CM^2

RAD. LEVEL	Isc	Voc	Imp	Vmp	Pmax	FF
*0	115.80	1026.10	109.40	859.90	94.07	0.792
*5E+10	112.90	996.80	106.50	836.80	89.12	0.792
*1E+11	111.50	984.40	104.90	821.70	86.20	0.785
*2E+11	110.00	969.40	103.20	807.20	83.30	0.781
*5E+11	107.40	943.40	100.70	773.10	77.85	0.768
*1E+12	104.80	919.10	98.20	743.20	72.98	0.758
*2E+12	100.90	889.70	94.20	712.90	67.16	0.748
*5E+12	93.00	842.30	86.10	663.80	57.15	0.730
*1E+13	83.10	799.10	76.40	625.70	47.80	0.720
1E+13/ANN(RT 1)	83.30	800.70	76.50	629.60	48.16	0.722
1E+13/ANN(RT27)	83.10	805.50	76.33	633.90	48.39	0.723

PROTON TEST 10.0 MEV NORMAL IRRADIATION
HRL GaAlAs Xw= 0.5 uM Xj= 0.5 uM 15 MIL BOX 119
Ta2O5 AR COATING
4/84

CELL AREA = 4.000 CM^2

RAD. LEVEL	Isc	Voc	Imp	Vmp	Pmax	FF
*0	115.70	1023.00	109.60	846.90	92.82	0.784
*5E+10	113.00	994.70	106.80	830.30	88.68	0.789
*1E+11	111.50	983.10	105.50	819.60	86.47	0.789
*2E+11	109.90	968.00	104.00	800.60	83.26	0.783
*5E+11	107.80	945.00	101.10	779.20	78.78	0.773
*1E+12	104.80	920.10	98.20	751.40	73.79	0.765
*2E+12	101.00	891.10	94.40	718.30	67.81	0.753
*5E+12	93.10	843.50	86.40	668.60	57.77	0.736
*1E+13	83.40	800.30	76.70	628.50	48.21	0.722
1E+13/ANN(RT 1)	83.70	802.50	76.80	631.00	48.46	0.721
1E+13/ANN(RT27)	83.03	806.10	75.63	643.60	48.68	0.727